EPJ manuscript No.
(will be inserted by the editor)

Independent isotopic yields in 25 MeV and 50 MeV proton-induced fission of ^{nat}U

H. Penttilä[1] [a], D. Gorelov[1], V-V. Elomaa[1], T. Eronen[1], U. Hager[1] [b], J. Hakala[1], A. Jokinen[1], A. Kankainen[1], P. Karvonen[1] [c], I. D. Moore[1], J. Parkkonen[1], K. Peräjärvi[2], I. Pohjalainen[1], S. Rahaman[1] [d], S. Rinta-Antila[1], J. Rissanen[1] [e], V. A. Rubchenya[13], A. Saastamoinen[1f], V. Simutkin[1], T. Sonoda[1] [g], C. Weber[1] [h], A. Voss[1], and J. Äystö[1] [i]

[1] University of Jyvaskyla, Department of Physics, P.O.Box 35 (YFL), FI-40014 University of Jyvaskyla, Finland
[2] STUK - Radiation and Nuclear Safety Authority, P.O. Box 14, FI-00881 Helsinki, Finland
[3] V. G. Khlopin Radium Institute, 194021, St. Petersburg, Russia

Received: date / Revised version: date

Abstract. Independent isotopic yields for elements from Zn to La in 25-MeV proton-induced fission of ^{nat}U were determined with the JYFLTRAP facility. In addition, isotopic yields for Zn, Ga, Rb, Sr, Zr, Pd and Xe in 50-MeV proton-induced fission of ^{nat}U were measured. The deduced isotopic yield distributions are compared with a Rubchenya model, GEF model with universal parameters and the semiempirical Wahl model. Of these, the Rubchenya model gives the best overall agreement with the obtained data. Combining the isotopic yield data with mass yield data to obtain the absolute independent yields was attempted. The result depends on the mass yield distribution.

PACS. 24.75.+i General properties of fission – 25.85.-w Fission reactions – 25.85.Ge Charged-particle-induced fission – 28.60.+s Isotope separation and enrichment

1 Introduction

A thorough characterization of the fission process requires a knowledge of the yield distributions of the fission fragments. In addition to understanding the fission dynamics, the data on yield distributions are important for optimising the production of neutron-rich nuclei in nuclear structure studies at existing facilities such as the IGISOL (Ion Guide Isotope Separator On-Line) [1] at the Accelerator laboratory of the University of Jyvaskyla, as well as simulating future ISOL-based radioactive beam facilities such as EURISOL [2]. Fission yield data are needed also for the development of the so-called Generation IV nuclear reactors [3].

The most complete description of the fission yield distributions is the *independent fission product yields* $Y(A, Z)$, the fractions of specific nuclides produced directly (not via radioactive decay of precursors) in fission [4]. Since the fission fragments evaporate neutrons in less than 10^{-15} s, they are not directly detected in experiments. The experimentally observed nuclei are *fission products*, defined as secondary fragments after the particle emission but before beta decay. Other fission yields are the *cumulative yields* - fractions of specific nuclides produced in fission, directly and via decay of precursors - the *chain yields* and the *mass (number) yields*. The chain yields are defined as the cumulative yield of the last member of the radioactive decay chain, the mass yields as the sum of all independent yields of a particular mass chain. The difference between the chain and mass yields results from the beta delayed neutron emission. The difference is significant only for few mass chains, in particular A=84,85,136 [4]. From experimental point of view it can be said that radiochemical methods (e.g. in ref. [5]) measure the chain yields, fission experiments in scattering chambers [6,7] where the

[a] *corresponding author:*penttila@jyu.fi
[b] *Present address:* Department of Physics and Astronomy, Michigan State University, East Lansing, Michigan 48824, USA
[c] *Present address:* Power Division, P.O. Box 100, FI-00048 Fortum, Finland
[d] *Present address:* Abbot Medical Optics Inc., 1700 East Saint Andrew Place, Santa Ana, California 92705, USA
[e] *Present address:* Fennovoima Oy, Salmisaarenaukio 1, FI-00180 Helsinki, Finland
[f] *Present address:*Cyclotron Institute, Texas AM University, College Station, Texas 77843-3366, USA
[g] *Present address:* Nishina Center for Accelerator Based Science, RIKEN, 2-1 Hirosawa, Wako, Saitama 351-0198, Japan
[h] *Present address:* Faculty of Physics, Experimental Nuclear Physics, Ludwig-Maximilians-Universität München, Am Coulombwall 1, D-85748 Garching, Germany
[i] *Present address:* Helsinki Institute of Physics, P.O.Box 64, FI-00014 University of Helsinki, Finland

mass determination takes place in hundreds of nanoseconds, measure the mass yields.

In the experiments described in this article the *independent isotopic yields of fission products* were established. The measured yields are independent with respect to beta decay. Because of the experimental reservations, the yields are determined relative to those of isotopes of the same element.

A measurement of the independent yield of a nuclide requires that it is observed and identified. A fission product can be recognised as an ion, or by following its radioactive decay. A major challenge is that over 500 different nuclei are produded in fission, of which about a half has a half-life shorter than 1 second. The large diversity of products limits the feasibility of the decay spectroscopy without pre-selection, which can be achieved by chemical (selection of Z) or physical means (selection of A with an isotope separator). The short-lived species form a technical challenge for both chemical and physical selection that cannot always be overcome. After separation, gamma ray spectroscopy is the most applicable for recognizing the decays; deducing the number of fission procucts from the gamma ray peak intensities requires good knowledge on the decay properties.

The ion guide technique [8,9] based mass separation is well suited for fission yield studies. It is universal in the sense it can produce an ion beam of any element within a few milliseconds. Fission yields have been determined by ion-guide based isotope separation combined with gamma-ray spectroscopy for proton-induced fission of ^{238}U in Jyväskylä [10–12], in Louvain-la-Neuve, Belgium [13–16], and in Sendai, Japan [17,18], for proton-induced fission of ^{232}Th in Sendai [19], for deuterium- and fast neutron-induced fission in Jyväskylä [12,20] and for alpha-induced fission of ^{238}U in Lyon, France [21].

Alternatively, the ions of fission products can be observed directly. Gas filled detectors around the fissioning target have been used in total (neutron-induced) fission cross section measurements [22,23] and fission product angular distribution measurements [24]. Their resolution is not however sufficient to identify all the fission products by Z and A. Measuring simultaneously the velocity (from the time-of-flight) and energy of the fission products allows determining the mass number of fission products [6, 7,25].

The fission products can be decisively identified on the basis of their mass. The mass resolving power of an ordinary isotope separator is seldom sufficient for this purpose. The Lohengrin recoil mass separator at ILL for unstopped thermal neutron-induced fission products [26] allows recognising the nuclear species up to Z $<$ 42 and consequently determining the independent yields for the light fission products; for heavy fission products, decay spectroscopic techniques have to be utilised.

During the last decade, Penning traps have become a widely used analysis tool in nuclear physics laboratories. One particular application of a Penning trap is to use it as a high precision mass filter. A mass resolving power (MRP) $m/\Delta m \approx 10^5$, provided easily with Penning traps, is sufficient to unambiguously identify most isotopes based on their mass. At the IGISOL facility [27,1] the ion identifying capability of JYFLTRAP [28] has been combined with the ion guide technique to produce a clean ion beam of any element. The combination allows the extraction of independent isotopic yield distributions. The method has been described in detail earlier in refs. [29–31].

In this article, the yield measurements of 25 MeV proton-induced fission of natural uranium are described, and the independent isotopic fission yields for elements from Zn (Z= 30) to La (Z=57) are given. In addition, a few isotopic yield distributions for 50 MeV proton-induced fission are presented. The data were obtained in experiments performed at IGISOL-3 [27] and completed later at IGISOL-4 [1]. A serious effort to convert the independent isotopic fission yield distributions to absolute independent fission yields in 25 MeV proton-induced fission is made.

2 Experimental techniques and data analysis

The independent isotopic fission yields were determined using a technique based on the unambiguous identification of the fission products by mass utilizing a Penning trap. The method is described in detail in ref. [29].

After the experiments described in ref. [29], the IGISOL facility has been updated to IGISOL-4 [1]. The fission yield measurements with 25 MeV protons were completed at the renovated facility. In the more recent measurements, an automated control of the dipole magnet of the IGISOL mass separator was employed. This has some impact on the way the experiments are executed, and, consequently, on the data analysis. In the new facility, better understanding of the appearance of the ion beams of the naturally occurring stable isotopes and their impact on the fission yield measurements has been gained. These findings are discussed in section 2.1.

Fission was induced by 1 - 4 μA beams of 25 MeV or 50 MeV protons from the K130 cyclotron. The target, a 10 mm by 50 mm piece of 15 mg/cm^2 thick uranium foil was located in the fission ion guide of the IGISOL mass separator [27,1]. The energy loss of protons in the target is 1.0 MeV at 25 MeV, and 0.6 MeV at 50 MeV, thus the fission is induced by practically monoenergetic protons. Natural uranium targets consists typically of 99.3 % of ^{238}U and 0.7 % of ^{235}U. The total proton-induced fission cross section for both isotopes is of the order of 1.4 barn at 25 MeV, thus, contribution from ^{238}U dominates the proton-induced fission yield disrtibution. The contribution of the neutron-induced fission can be considered negligible. The fast neutrons from fission induce of the order of $10x10^6$ fissions per each μC of primary proton beam, which needs to be compared to $20x10^9$ proton-induced fissions per μC of primary proton beam. The target is so thin that the fission neutrons escape before they are slowed down to thermal energies. The most significant source of thermal neutrons is the beam dump 3 meters downstream of the target. An upper limit estimation of thermal neutron flux yields to less than 1000 thermal neutron-induced fissions of ^{235}U in the ^{nat}U target per μC of proton beam.

In the ion guide technique [8,9], the reaction products are ionized in the nuclear reactions, fission in this case. They recoil out of the target as ions, which are stopped in helium buffer gas. The charge state of the originally highly charged ions lowers rapidly, until the fission products cannot strip any more electrons from helium atoms. The majority of the reaction products stopped in helium remain as 1+ ions long enough to be transported with the helium flow to a differential pumping section, where they are guided by a sextupole ion beam guide, SPIG [32], to a magnetic mass separator. A self-focusing 55° Scandinavian type dipole magnet is used to disperse the masses with a MRP $m/\Delta m \approx 500$. At IGISOL-3, the ions with mass number A were selected by a 7 mm wide slit, and at IGISOL-4 with a variable slit width set to 10 mm. The selected ions are directed to a linear quadrupole radiofrequency cooler and buncher (RFQ) [33–35], where they were collected for up to a few hundreds of milliseconds.

The collected ions are released as a 10 μs long bunch that is directed to the cylidrical double Penning trap JYFLTRAP [28], which consist of two traps within the same 7.0 T superconducting magnet separated by a 50 mm long, 2.0 mm in diameter (1.5 mm at IGISOL-4) channel. The ion bunch is captured in the first of the traps, called the purification trap. The purification trap, filled with low pressure helium, can be used as a high MRP ($\geq 10^5$) filter for the ions. The filtering is done by applying multipole RF fields to the azimuthally 8-fold split ring electrode at the center of the trap.

The movement of the ions in the Penning trap consists of three eigenmotions: axial motion along the magnetic field, and two radial motions perpendicular to it. The lower frequency magnetron motion, with frequency ν_-, is essentially mass independent, while the higher frequency reduced cyclotron motion, ν_+, exhibits a mass dependence. The sum of the frequencies is called cyclotron frequency ν_C, that satisfies the equation

$$\nu_- + \nu_+ = \nu_C = \frac{1}{2\pi}\frac{q}{m}B, \qquad (1)$$

where q and m are the charge and mass of the ion, and B is the magnetic field [36].

The ion purification, i.e., selecting the ions with the mass of interest, starts with an initial cooling period. Next, a dipolar RF field is applied to the Penning trap ring electrode at the magnetron frequency ν_-. It excites the magnetron motion without affecting the other eigenmotions. Since magnetron motion is mass independent, all ions are moved to an orbit away from the trap center. The amplitude of the dipolar field is chosen such that the radius of the orbit will be so large that no ion can pass the narrow channel between the purification trap and the second trap upon the release from the purification trap.

After the dipolar excitation, a radial quadrupole RF field with the cyclotron frequency ν_C of interest is applied. This causes a coupling of the radial eigenmotions and a conversion of the magnetron motion to the reduced cyclotron motion for the ions that satisfy equation 1. As the result, the magnetron radius of the selected ions decreases. This increases their reduced cyclotron motion radius momentarily, but the collisions with the buffer gas will finally decrease also the ν_+ amplitude, due to which the ions of interest are centered in the trap and can be extracted out of the purification trap through the aperture. With this technique, $m/\Delta m \approx 10^5$ is reached. The purification process is described in detail in refs. [37,28,38].

The ions were counted with a multichannel plate (MCP) detector located at ground potential outside of the trap magnet. Since the trap is located at 30 kV high voltage, the released ions are accelerated over this voltage. A detection efficiency of ≈ 60 % is, as compared with ≈ 20 % for a few keV ions. Examples of the resulting spectra that are used to determine the fission yields are shown in figure 1. Strictly speaking, they are cyclotron frequency spectra, inversely proportional to mass. As a good approximation, they can be considered as mass spectra, and hence called such in the following.

Since the ionization mechanism is the fission itself, the independent fission yield of an isotope is directly proportional to the intensity of the corresponding peak in the mass spectrum. Since the time from fission to the ion detection was relatively long, from 341 ms up to 1300 ms, an appropriate radioactive decay loss correction needs to be applied for the most short-lived isotopes. The fission yield distributions can be extracted from the corrected yields. Since both the ion guide efficiency and the transmission efficiency through the RFQ and the Penning trap can depend on the chemical properties of the isotope [39, 30], usually only the isotopes of the same element were compared.

Each measured mass spectrum was associated to a reference mass spectrum. In the experiments at IGISOL-3, the reference was recorded before and after each mass scan, and, if possible, the same reference isotope was used for all isotopes of a certain element. The mass spectra were measured in an irregular sequence to avoid any systematic drift of experimental conditions that may skew the determined distribution of fission yields. In addition to the mass spectrum, a history spectrum showing the count rate variation along the course of the experiment was generated. These history spectra could be used to correct for element-independent fluctuations of the mass separated beam intensity [29]. These fluctuations turned out to be mostly due to the instability of the manual control system of the dipole magnet[29]. Later, a more stable computer control was implement, which also allowed more frequent swapping to and from the reference mass number. In the experiments at IGISOL-3, a mass spectrum consisted of 20 - 100 consecutive Penning trap frequency scans, each scan having one ion bunch per a frequency point. Reference mass spectra typically consisted of 20 - 50 frequency scans.

In the experiments at IGISOL-4, the fast computer control allowed a change of mass number after every three or four frequency scans, until a sufficient number of scans (typically 30) was performed, see figure 2. This difference has some impact on the analysis of the yields and the choice of the reference. In comparison to earlier measure-

ments, 2 - 4 reference isotopes were used for each element. The choice of the reference isotopes is discussed later in section 2.2.

It is worth noting that the yields were determined from mass spectra such as shown in figure 1, each spectrum having several peaks. In order to have better control over the measurements, each spectrum had to have at least one mass peak with a sufficient yield. As an example, the highest rate of ^{111}Pd ions is less than 1 ion per bunch. At such a rate it is difficult to notice any variations of the count rate, for example, due to primary beam fluctuation. The ^{111}Rh mass peak in the same spectrum provides a more sensitive monitor for the stability of the yield. A sufficiently wide frequency range also allows the determination of yields of several nuclides simultaneously.

In the analysis, the number of counts in a mass peak was used as the measure of its intensity. This choice is discussed in detail in ref. [29]. As seen from figure 1, there are very few background counts in the spectra, so there was usually no need for background subtraction. Nevertheless, the mass resolving power is an important aspect in the analysis of the mass spectra. In mass numbers $A < 125$, a MRP of the order of 10^5 is sufficient and overlapping of mass peaks is rare. For the heavier fission products, a higher mass resolving power is needed to properly separate the mass peaks due to various reasons:

- the valley of beta stability bends towards more neutron rich nuclei
- the fission products in the heavy mass peak are on the average less neutron rich than in the light mass peak (charge polarization) which brings the distributions closer to the valley of stability
- above $A = 130$ the mass parabola is wider and shallower than below, bringing the masses within each isobar closer to each other
- the mass resolving power of the Penning trap gets lower at higher masses. The resonance frequency ν^* of an isotope is inversely proportional to its mass, while the resonance width $\Delta\nu^*$ remains constant. Thus, for the same mass difference Δm the frequency difference $\Delta\nu^*$ is smaller for heavier isotopes.

The most difficult region for resolving the mass peaks is at $A = 128$ - 136. The maximum of fission yield falls in between the stable isotopes and the doubly magic ^{132}Sn, whose increased binding energy due to nuclear structure reduces its mass close to that of stable nuclei. The mass differences are small and as such proper resolving of the mass spectra is challenging. The presence of the natural xenon isotopes, used as a mass calibration gas at IGISOL-3, were harmful for tin, antimony and caesium measurements, and made it impossible to determine the yields of tellurium and iodine. While the space charge due to the most abundant isotopes ^{129,131,132}Xe prevented any measurements whatsoever, even the less abundant isotopes reduced the resolving power enough to make the mass spectra irresolvable, except for the mass peaks of isotopes furthest from stability. At IGISOL-4, where the use of natural xenon as a calibration gas was avoided, the situation was better but resolving the mass spectra was still quite challenging.

After determining the ion rate after the JYFLTRAP Penning trap, the aforementioned corrections due to radioactive decay and count rate fluctuations were applied to the isotopic yields. For details, see ref. [29]. The isotopic yields are determined from the ratios of the count rates of the reference isotope and the isotope of interest. The normalised isotopic yields are given in tables 3 - 12. The uncertainty includes both the statistical uncertainty as well that due to the applied corrections.

2.1 Stable isotopes

Since the technique is based on ion counting, it allows in principle determination of the fission yields of long lived and stable isotopes as well as the radioactive ones. Some stable isotopes are produced directly in fission. In 25 MeV proton-induced fission of natural uranium studied in this work, such isotopes include e.g. ^{82}Se, ^{86}Kr, ^{96}Zr, ^{100}Mo, ^{110}Pd, ^{116}Cd, ^{122,124}Sn, ^{128,130}Te and ^{137,138}Ba. Determining the independent fission yield of stable isotopes is however challenging in practice, since stable isotopes, not directly produced in fission, are ionised in the IGISOL target area and observed in the mass spectra as well. Their presence can be seen in figure 1, where the isotopes of cadmium appear in mass numbers $A = 110$ - 113. The vast majority of cadmium isotopes produced in fission has a mass number $A >115$. In addition to cadmium, the ions of stable isotopes of Ge, As, Se, Br, Kr, Rb, Sr, Mo, Cd, In, Sn, Te, I and Xe have been observed in the measurements. In the following, these ions are called *stable background*, if it is necessary to distinguish them from the stable isotopes produced in fission.

The origin of all stable background is not yet fully understood. A very small amount of material is needed, since the intensity of the stable background ion beams is in most cases less or of the same order of magnitude than that of fission products. Of the observed elements, gaseous krypton and xenon are present as impurities in the helium gas. They are ionised by the fission fragments and scattered primary beam, and also by the beta and gamma radiation from the decay of the fission products stopped in the ion guide. Xenon was earlier used for the mass separator calibration and intentionally added to helium. In more recent experiments use of xenon has been avoided. Indium wire is used for gas sealings. Several trace elements, including e.g. cadmium, molybdenum, arsenic, selenium, antimony, tin, zinc and lead are present in human sweat [40], although separator parts should not have been handled without gloves during mounting.

The most severe impact of the stable background ions on the yield measurements is that some are produced so abundantly that the space charge they build in the Penning trap reduces its transmission. The isotopic yields of germanium and gallium are shown in figure 3. The yield is reduced at A=79 and A=81 for both elements, which is due to the presence of stable bromine. In the case of bromine, the intensity of the background bromine beam

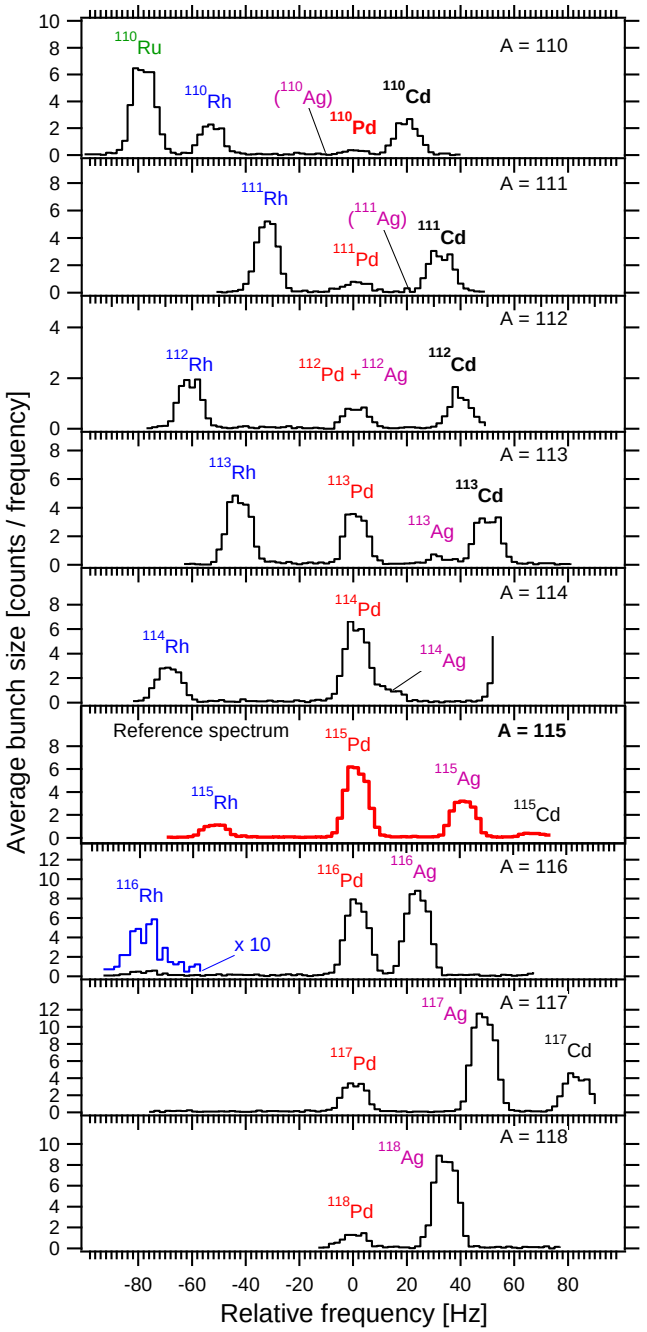

Fig. 1. Sequence of mass spectra used to determine the isotopic yields of Pd isotopes. The horizontal scale is the Penning trap excitation frequency, so the mass of the isotopes increases to the left. The frequency in all spectra is given relative to the palladium mass peak position. The vertical scale is the average number of ions per bunch. A low rate in the A=112 mass spectrum is due to transmission efficiency fluctuation, which is corrected for in the calculation for the isotopic yield. The mass peaks labeled in bold are those of stable isotopes. The stable Cd isotopes are not fission products but impurities, while most of the stable ^{110}Pd seems to be fission products. The same mass spectra could also be used to determine isotopic yields of several Rh and Ag isotopes.

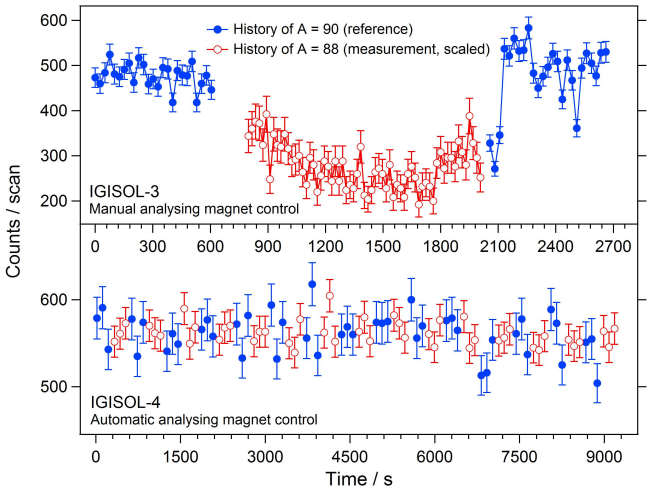

Fig. 2. Histories of a fission yield measurement with the same isotope-reference pair at IGISOL-3 (top) with manual and at IGISOL-4 (bottom) with automated dipole magnet control. The history of A=88 has been scaled in such a way that it mimics the reference A=90 yield, see [29,31] for details. The total measurement time is longer at IGISOL-4 because of higher frequency resolution and longer frequency range of each mass scan.

is several orders of magnitude higher than that of any fission products. A similar reduction has been observed because of Rb (A=85,87; not in current data), I (A=127; IGISOL-4 only) and Xe (A=131,132,134; IGISOL-3 only). The intensity of the stable background beams varies between measurements, and the space charge due to them is not always sufficient to influence the trap transmission.

An effort was also made to estimate the intensity of the stable background beam and subtract its contribution from the yield of stable isotopes originating from fission. The starting point for each element was the ion yield of a stable isotope that certainly was not produced in fission. The rate of other stable background isotopes was estimated from the natural abundance ratios. However, it turned out that the intensity of the background did not always follow the natural abundances, which makes the question of their origin even more puzzling. From the current point of view of fission yield measurements it is important that their presence is recognized and taken into account in the analysis.

2.2 Choice of reference isotopes

2.2.1 IGISOL-3

In the experiments performed at IGISOL-3, typically one isotope of each element was selected as a reference isotope. The requirements for an *optimal* reference isotope were

- the mass peak of a reference isotope should not overlap with any other mass peaks
- the mass peak should be a single peak, not consisting of two or more close-lying isomers

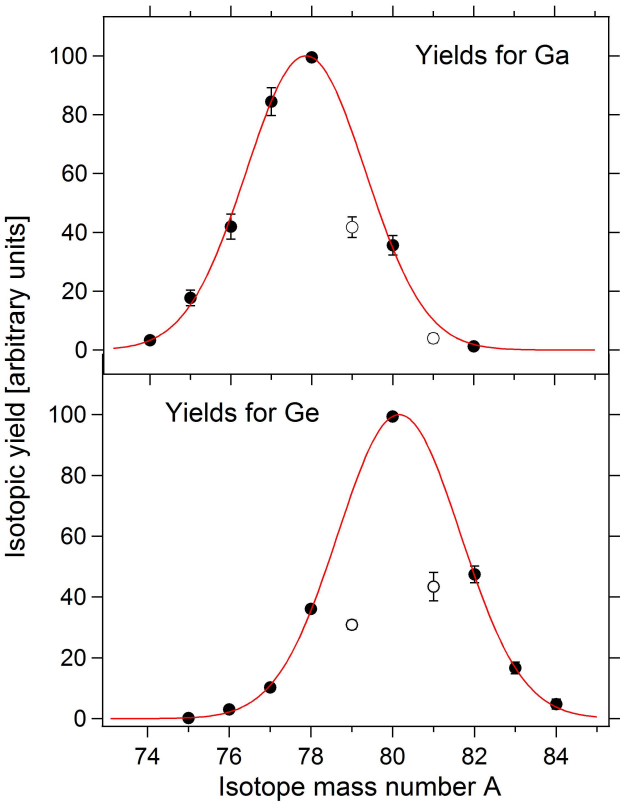

Fig. 3. Determined yield distributions of germanium and gallium isotopes. The height of the Gaussian fit to the data points indicated by solid circles is normalised to 100. The open circles show the measured yield in mass numbers A = 79 and$A$ = 81 that fall below the expected value. An equal drop is seen also for As in A = 81 and for Zn in A = 79. The effect is due to space charge from natural ^{79,81}Br ions that reduces the transmission through the Penning trap.

– the half-life of the reference isotope should be relatively long or sufficiently well known to avoid uncertainty due to decay correction.
– the reference isotope should (usually) be close to the maximum of the isotopic yield distribution.

In practice, some criteria had to be relaxed. This was related to the optimal use of the available beam time resources. Figure 1 shows the mass spectra used to determine the fission yields of palladium. The yields of several rhodium and silver isotopes can be deduced from the same spectra. The spectra shown in figure 1 are not sufficient to determine the whole isotopic yield distribution for rhodium and silver. The remainder was determined against a reference other than A = 115, which allowed a simultaneous measurement of the yields of the next elements. The way to combine the measurements against different reference isotopes is described below.

The region around mass number A = 130 has isobars with very small mass differences, resulting in many overlapping mass peaks. The reference isotopes for elements from xenon to lanthanum were thus chosen relatively far from stability. Some overlapping of reference mass peaks could not be entirely avoided, since the choice also had to balance with the lower yield and shorter, less well known half-life of the isotopes far from stability.

Reference isotopes with isomers could neither be totally avoided. When the half-lives of isomers are long enough, tens of seconds or longer, the effect of the isomeric ratio to the deduced yields is however negligible.

The last criterium, having the reference isotope close to the maximum of the yield is related to achieving appropriate counting statistics faster for the reference. However, the highest possible yield for the reference is not always optimal. Low yield of the isotopes far from stability can be boosted with higher primary beam intensity. The reference isotope rate needs to be measured with the same primary beam intensity to have the same conditions in the ion guide. The counting rate of the reference isotope is limited by the pile-up limit in the MCP detector [29], which partly dictates the upper limit for the primary beam intensity. The other limiting factor is the total amount of ions (space charge) in the Penning trap, which is less of a concern than the pile-up limit, provided any contaminating stable ions are not involved. Therefore, isotopes far from stability can often be more effectively measured against a nearby isotope with a similar count rate and using more intense primary beam.

Usually, a reference isotope of the same element was used. On some rare occasions, the intensity of the appropriate reference isotope could not be determined from the reference spectrum. In such cases, each separately discussed in section 3, an isotope of a different element was used as a reference. Even though the transmission efficiency is different for different elements, the relative efficiencies change slowly, as shown in ref. [30]. Comparison against any element in the reference spectrum thus gives the same shape of the yield distribution. In addition to Zr, Nb and Mo isotopes discussed in ref. [30], the stability of the relative transmission efficiency has been investigated by comparing the ratios of ^{123}In/^{123}Sn, ^{96}Sr/^{96}Y and ^{74}Zn/^{74}Ga in the reference mass spectra. The variation of these ratios stayed within the statistical fluctuation during the length of the experiment - Zn/Ga ratio for nine hours, and Sr/Y ratio for four hours.

For the final result the isotopic yields are further normalized to 100 corresponding to the height of a Gaussian fit to their distribution. This normalization makes it easier to compare different distributions since it is less arbitrary than setting some reference isotope to 100. In addition, the Gaussian fits are utilized in combining the isotopic yields measured against different reference isotopes. This is explained in more detail below.

2.2.2 IGISOL-4

In the measurements at IGISOL-4 a slightly different approach to the selection of the reference isotopes was adopted.

Unlike at IGISOL-3, the dipole magnet used to select the mass number A of the ions collected in the RFQ, was computer controlled. This allows changing between the measured mass and the reference mass in significantly

shorter intervals than before. In a typical measurement the reference mass number was scanned over the range of interest three times. Then the mass number was changed, which took 10 - 20 seconds, depending on the magnitude and direction of the magnetic field change. The mass of interest was then scanned three times. This was repeated until sufficient statistics was reached. A typical yield measurement consists of 30 - 50 frequency scans for both the mass of interest and the reference mass, see figure 2.

At IGISOL-4, the mass difference between the studied and the reference isotope was minimised, firstly to reduce the dipole magnet current change between the isotopes, and secondly, to maintain a similar ion counting rate for both isotopes (see discussion above).

In each IGISOL-4 measurement, one reference was used for a set of 3 - 4 isotopes. Then, a new subset with another reference was started. The subsets overlapped in at least one, preferably in two mass numbers. If necessary, a third and even fourth subset was collected to cover the whole isotopic yield distribution.

The yield subsets were combined so that the reference of a subset was matched to the yield in the previous subset by multiplying the subset by an appropriate factor. In a typical case of bromine isotopes the ^{86}Br set was multiplied by 4.178, see table 1. Since the uncertainty of the next reference isotope yield is zero, its final uncertainty comes from the measurement against the previous reference (for ^{86}Br against ^{84}Br). A weighted average is used for other overlapping isotopes (^{85}Br in the case of Br isotopes). The ^{88}Br set is multiplied by $4.178 \times 0.91 = 3.815$ to adjust the reference isotope ^{88}Br and so on, if there was a fourth reference set.

In some cases all subsets could not be linked to a reference isotope, see for example the case of tellurium isotopes in table 1. If the subsets had only one common isotope, the joint subset was multiplied by an appropriate factor, but now the factor has an uncertainty that is quadratically added to the uncertainty of the isotopes in the multiplied set. If there were two common isotopes, as in the case of second and third tellurium reference subsets, the multiplication factor is determined so that the yield of one isotope is above and the yield of another below the value in the previous subsets. One adjusted yield needs to be an equal amount above the established value than the other is below. This equal amount is however not in absolute yield units but in the total uncertainty of the difference. In the case of tellurium, ^{131}Te and ^{133}Te subsets (the first and the second reference set in table 1) are first combined as above in the case of bromine by multiplying the ^{133}Te set by 0.93. This result yields 21.72 ± 0.70 and 14.40 ± 0.57 for ^{135}Te and ^{136}Te, respectively. The third, ^{137}Te set is then multiplied by a such factor that the yield of ^{135}Te in the third set becomes as much above the combined yield of ^{135}Te as ^{136}Te is below. Such a factor is 0.06183: it gives 24.86 ± 1.49 and 12.61 ± 0.75 for the yields of ^{135}Te and ^{136}Te, respectively. The difference of ^{135}Te yields between the combined ^{131}Te and ^{133}Te set and the ^{137}Te set is (21.72 ± 0.70) - (24.85 ± 1.48) = -3.13 ± 1.64, which means that the yield of ^{135}Te in the combined set is 1.9σ below the yield in the ^{137}Te set. Respectively, the yield of ^{136}Te is (14.40 ± 0.57) - (12.61 ± 0.75) = 1.79 ± 0.94, 1.9σ above the ^{137}Te set. For the final yield of ^{135,136}Te the weighed averages (22.29 ± 0.64 and 13.74 ± 0.46) are used.

As a last step, the yields are normalised so that the height of a Gaussian fit to each isotopic distribution equals 100. These values are shown for bromine and tellurium in the last column of table 1. These are also the IGISOL-4 yields shown in tables 3 - 11.

Auxiliary data. There were some additional data collected at IGISOL-4 that can be used to determine the isotopic yields of elements that are heavier than lanthanum. Consecutive mass scans up to A= 157 were performed to locate the mass peak regions. Proper yield measurements against a reference mass spectrum were made only up to A = 142. Such spectra were collected in three relatively short (2-3 hours) periods. Fission yield distributions from Te to Pm can be constructed from these data by taking the mass peak intensities and correcting them for the decay losses. It is relatively safe to assume that the conditions did not vary too much during the scan. In addition, the same mass spectra were collected three days apart with slightly different trap settings. The ratio of the extracted yields from the two separate measurements vary less than the statistical uncertainty.

2.3 Gaussian fit of the isotopic yield distributions

A Gaussian fit was used to determine the centroid A_p and width σ_A of each yield distribution. The fit parameters - the centroid position A_p, the height Y and the width σ_A - were not fixed, and the fit was weighted with the uncertainty of the data points. Since the uncertainty of the yield for the reference isotope is set to zero, the fitted Gaussian must go through the reference yield data point. This removes one degree of freedom from the fit, which is taken into account in the calculated quality of the fit, $\tilde{\chi}^2$.

Some data sets were insufficient in such a way that the Gaussian fit did not converge before either A_p or σ_A was fixed on the basis of a priori knowledge. These are discussed case by case in section 3.

The height Y of the fitted distribution was used to normalise the yield distributions. In particular, when the yields were determined against two different reference isotopes, the Gaussian fits were used to normalise the data before combining the experimental values. Similar normalisation was also utilised in combining the IGISOL-3 and IGISOL-4 measurements. This is described in the next section.

2.4 Combining yield measurements

The result of the analysis is a ratio between the count rates in the mass peaks of the isotope of interest and its reference isotope. The same isotope could be measured

Table 1. Combining bromine and tellurium yield subsets in IGISOL-4 measurements. 25 MeV proton-induced fission, see text for the details.

Isotope	Reference sets			Combined	IGISOL-4
	First	Second	Third	yield	yield
^{83}Br	19.6 ± 2.3			19.6 ± 2.3	3.74 ± 0.44
^{84}Br	100			100	19.1
^{85}Br	290.5 ± 10.3	64.8 ± 2.9		282.2 ± 7.9	53.9 ± 1.5
^{86}Br	417.8 ± 12.0	100		417.8 ± 12.0	79.8 ± 2.3
^{87}Br		132.8 ± 4.8	129.9 ± 5.8	528.1 ± 14.9	100.9 ± 2.9
^{88}Br		91.3 ± 4.3	100	381.5 ± 18.0	72.9 ± 3.5
^{89}Br			69.7 ± 4.7	265.9 ± 18.0	50.8 ± 3.5
^{90}Br			20.9 ± 3.1	79.7 ± 11.9	15.2 ± 2.3
^{129}Te	68.0 ± 1.7			68.0 ± 1.7	67.8 ± 1.7
^{130}Te	-			-	
^{131}Te	100			100	99.8
^{132}Te	-			-	
^{133}Te	93.0 ± 2.8	100		93.0 ± 2.8	92.8 ± 2.8
^{134}Te		66 ± 13		61.4 ± 12.1	61 ± 12
^{135}Te		23.36 ± 0.75	402 ± 24	22.29 ± 0.64	22.25 ± 0.62
^{136}Te		15.48 ± 0.61	204 ± 12	13.74 ± 0.46	13.71 ± 0.45
^{137}Te			100	6.18 ± 0.37	6.17 ± 0.37

against two (in a few cases even three) different reference isotopes. Only in a very few cases, the yield measurement against the same reference isotope was repeated. Usually this was due to technical problems, and all other measurements but one can be simply discarded. Finally, there are three different, equally qualified yield values for ^{106}Nb against ^{101}Nb, and two different values for ^{99}Zr, ^{99}Nb and ^{99}Mo against the respective A=101 isotope in 25 MeV fission. The final yield is the weighted average of different values.

Some yield distributions were measured with respect to two equally significant reference isotopes. For eight elements - As, Se, Br, Rh, Ag and Cd in 25 MeV and for Rb and Cs in 50 MeV proton-induced fission - there are two partly overlapping yield distributions, both consisting of at least four isotopes. These distributions were combined after they had been normalised using Gaussian fits. In the following, the "yield distribution determined against a reference isotope ^{A}Z" is called "^{A}Z set" for short.

A Gaussian shape was fitted to the different reference isotope sets. The centroid A_p and the width σ_A of the fit are given in table 2. Since both sets describe the same isotopic yield distribution, A_p and σ_A of the fit should be the same. Typically, the centroids are in agreement; for ^{85}Br set the fit does not however converge without fixing the centroid. In the widths there is more disagreement: those of selenium sets differ as much as 1.7σ, which is still statistically plausible, but the disagreement between cadmium sets is over 4σ.

The height of the fit was used to scale the yield sets before combining them. The experimental yields were scaled so that the fits have equal height. The relative uncertainty of the fitted height Y, δY, was quadratically added to the uncertainty of the scaled yields. The distributions were merged using a weighted average for the overlapping yields. Figure 4 displays the procedure for rhodium yields.

The method of constructing the yield distribution from the reference sets at IGISOL-4 is described above in section 2.2.2. The final yield distributions of IGISOL-4 measurements are also normalised so that the height of a Gaussian fit to the distributions equals 100. Whenever the isotopic yield distribution was measured at both IGISOL-3 and IGISOL-4, the results are combined using weighted average of the overlapping yields. Before combining, the relative uncertainty of the height Y of the Gaussian fit to the yield distribution was quadratically added to the uncertainties of the experimental yield values. Finally, the combined yield distribution was fitted with a Gaussian and the fit height normalised to 100.

3 Results

The obtained independent yields in 25 MeV proton-induced fission are given in tables 3 - 11 and the yields in 50 MeV proton-induced fission in table 12. Yields are normalised so that the height of a Gaussian fit to each isotopic distribution equals 100. Suspicious values are given in parenthesis. An interpolated yield is given for the missing or suspicious yields in square brackets. A yield value without an uncertainty is that of a reference isotope. If the final yields were obtained by combining two distributions (see section 2.4), an uncertainty was assigned also to the yields of the reference isotopes in this process. For 14 elements only one reference isotope was used. These reference isotopes, whose yield uncertainty is assigned to zero, are

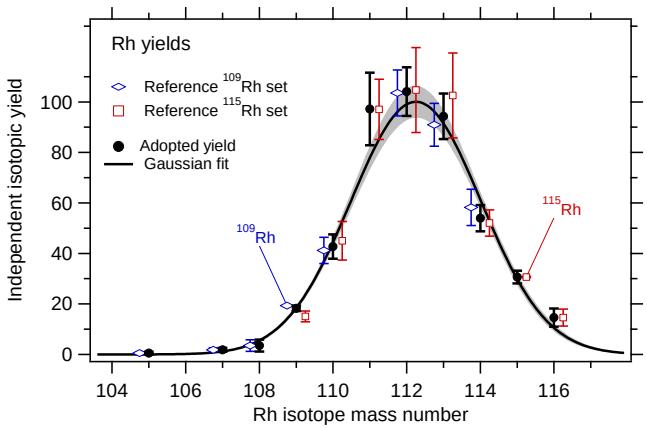

Fig. 4. The isotopic yield distribution of Rh determined against ^{109}Rh (^{109}Rh set, diamonds, offset left from the mass number for clarity, blue online) and ^{115}Rh (^{115}Rh set, squares, offset right, red online). The yields are scaled so that the height of a Gaussian fit to both sets equals 100. The scaled sets are combined as described in the text. For the final isotopic yields the combined yields are fitted by a Gaussian, whose height is normalised to 100. In case of Rh, this last normalisation shifts the values only by ≈1 %. For clarity, only the Gaussian fit to the final values is shown. The shaded area represents the 1σ confidence band of the fit.

Table 2. Centroids and widths of the 25 MeV proton-induced isotopic fission yield distributions for Se, Br, Rh, Ag and Cd for different reference isotope sets. These are weighted fits of a Gaussian shape $y(A) = Y\ e^{-(A-A_p)^2/{\sigma_A}^2}$ where A_p, Y and σ_A are free fit parameters unless otherwise noted.

Z	Ref	Centroid	Width	$\tilde{\chi}^2$
Se	^{80}Se	84.46 ± 0.10	1.44 ± 0.09	0.983
	^{85}Se	84.30 ± 0.26	1.69 ± 0.14	2.407
	comb	84.63 ± 0.08	1.59 ± 0.05	4.239
Br	^{85}Br	86.82 ± 0.13	1.97 ± 0.24	0.356
	^{89}Br	86.82 †)	1.92 ± 0.02	0.178
	comb	86.83 ± 0.11	1.91 ± 0.08	0.139
Rh	^{109}Rh	112.21 ± 0.13	1.77 ± 0.09	0.664
	^{115}Rh	112.30 ± 0.05	1.75 ± 0.07	1.983
	comb	112.25 ± 0.05	1.77 ± 0.05	1.015
Ag	^{115}Ag	117.53 ± 0.11	1.71 ± 0.09	1.094
	^{119}Ag	117.49 ± 0.07	1.79 ± 0.05	1.528
	comb	117.57 ± 0.04	1.75 ± 0.04	1.401
Cd	^{119}Cd	119.96 ± 0.03	1.72 ± 0.03	1.310
	^{123}Cd	120.12 ± 0.24	2.35 ± 0.14	0.608

†) fixed centroid position

^{76}Zn, ^{78}Ga, ^{82}As, ^{96}Sr, ^{96}Y, ^{101}Zr, ^{101}Nb, ^{101}Mo, ^{109}Tc, ^{109}Ru, ^{115}Pd, ^{131}Te, ^{141}Ba and ^{141}La.

The elements from strontium to cadmium (38 ≤ Z ≤ 48) were measured only at IGISOL-3. Zinc, gallium, tellurium and iodine (Z = 30,31,52,53) were measured only at IGISOL-4. For elements heavier than lanthanum (Z = 57) there is only a partial measurement at IGISOL-4. For xenon, the IGISOL-3 and IGISOL-4 distributions are so different that they could not be combined.

The results requiring further remarks are discussed in more detail in the following.

3.1 25 MeV proton-induced fission

Zinc and gallium

Isotopic yield distributions of zinc and gallium were measured at IGISOL-4 only.

The presence of a significant amount of natural ^{79,81}Br ions reduces the transmission through the JYFLTRAP severely in mass numbers$A = 79$ and $A = 81$. The experimental fission yields in these mass numbers could thus not be determined. In table 3 the interpolated yield is given for ^{79}Zn and ^{79,81}Ga in square brackets.

The yields of Zn isotopes have been normalised with a fit to all measured isotopes, even though ^{74,75}Zn can not be properly fitted with the same Gaussian distribution. If either of them is excluded from the fit, the fit improves significantly. Excluding ^{75}Zn does not significantly change the width of the yield distribution (1.30 ± 0.06), while excluding ^{74}Zn leads to very narrow distribution (1.12 ± 0.07) that clearly differs from neighbouring Ga and Ge (1.474 ± 0.033 and 1.501 ± 0.014, respectively). On the other hand, the yield of ^{75}Ga is deduced from the same mass spectra, and the Gaussian fit of the independent yield distribution of gallium with both ^{74,75}Ga can be performed without difficulty. There is however a considerable doubt that the experimental yield 69.6 ± 5.4 for ^{75}Zn is too low and needs to be remeasured. The interpolated values are given for both ^{74,75}Zn in table 3 in square brackets.

Germanium

For Ge, the measurements were made both at IGISOL-3 and IGISOL-4. The measurements are in excellent agreement.

The presence of the natural Br ions prevents determining the yields of ^{79,81}Ge.

The stable isotope ^{76}Ge is produced directly in fission. The production of the next stable germanium isotope, ^{74}Ge, is 40 times higher than that of radioactive ^{75}Ge, which indicates that natural germanium is ionised. The fission yield of ^{76}Ge was deduced by subtracting the natural yield, which was estimated from the abundance ratio of ^{74}Ge and ^{76}Ge. As discussed above, the stable isotope beam intensities do not always seem to follow the natural abundances. In the case of ^{76}Ge, the subtracted value agrees with the value interpolated from ^{75,77}Ge yields.

Arsenic

Arsenic ions have a lower transmission through JYFLTRAP than the neighbouring elements. Therefore, the arsenic yields typically have lower statistics and thus a larger uncertainty than the other elements whose yield are determined in the same mass spectra. Although the arsenic yields were determined from the measurements at IGISOL-3, these data have been omitted. The precision of the IGISOL-4 measurement for arsenic is so much better that it solely determines the final yields, if the results are combined. Nevertheless, the IGISOL-3 data is not in disagreement with the newer IGISOL-4 data.

Selenium

At IGISOL-3, the selenium yields were determined against ^{80}Se and ^{85}Se. ^{78}Se, ^{80}Se and ^{82}Se are stable isotopes, with natural abundances of 23.6, 49.9 and 8.9 %, respectively. It was however not realized during the experiment that natural selenium can be ionised at IGISOL. ^{80}Se was used as a reference, since it allowed the determination of selenium yields from the same mass scans as germanium up to ^{86}Se. The potential problem of the natural ion as a reference is that the ionisation mechanism is not the same as for the fission products and the ionisation efficiency can change. The ^{80}Se set is however in agreement with the ^{85}Se set (table 2).

The fission yield of the stable ^{82}Se was estimated by subtracting the contribution of natural selenium based on the natural abundances and yield of ^{80}Se. ^{82}Se yield could not be interpolated, since the yield of ^{81}Se was reduced due to ^{81}Br. The extrapolated yield, based on the Gaussian fit to $^{83-89}$Se, is 33 $\pm$ 5. This value is in agreement with the ^{82}Se yield of 28.8 $\pm$ 8.8 determined at IGISOL-3.

Bromine

At IGISOL-3, the bromine yields were determined against ^{85}Br and ^{89}Br. In addition, the yield of ^{84}Br could be estimated from the yields of ^{84}Br and ^{85}Br against ^{80}Se. The Gaussian fit of the ^{89}Br set did not converge before fixing the centroid of distribution to that of the ^{85}Br set (see table 2).

Krypton

Krypton ions are among the most reactive species in the gas-filled traps: they neutralise easily.

The krypton yield measurement at IGISOL-4 covered $^{87-91}$Kr with ^{88}Kr as the primary and the only reference. The directly obtained yields were scattered without any obvious logic. Since the whole isobaric chain was measured for each mass, the krypton yields could be analysed also via the isobaric yield distributions. In figure 5 the isobaric yield distributions for $A = 88$ and $A = 89$ are shown. The yield of krypton is clearly reduced in both isobars. Excluding krypton and assuming no significant difference in the behavior between the other elements, the isobar can be fitted with a Gaussian. The stable ^{88}Sr is background and not included in the fit. Incidentally, the width of these fits, shown as a dashed curve in figure 5, is $\sigma_Z \approx 0.73$, only slightly more than the typical 0.69 - 0.71 average of the charge distributions quoted in [12,18,41]. In addition, the charge distribution centroids agree with the ones measured for 25 MeV proton-induced fission in [12,18]. The open circles in figure 5 indicate the yield expected for the krypton isotopes on the basis of interpolation.

It is seen from figure 5 that a larger fraction of ^{89}Kr ($\approx$ 90 %) is neutralised than ^{88}Kr ($\approx$ 70 %). The isobars are deduced from the yield measurement of $A = 89$ isotopes against $A = 88$ isotopes as reference. Furthermore, since ^{88}Kr was used as a reference, there were several runs of $A = 88$. All measurements showed the same 70 % reduction of ^{88}Kr as compared with the other elements. This repeatiability shows that the difference between the krypton isotope transmission was not due to random fluctuation.

Since krypton isotopes have same chemical behavior, there must have been a difference in circumstances after the mass number selection with the dipole magnet. The selection and amount of atomic ions in the RFQ and the Penning trap is very similar for both masses. The only possible stable atomic background in $A = 88$ is ^{88}Sr and in $A = 89$ ^{89}Y, neither which were seen in the mass spectra. Still, intense molecular ion beams could have been present. The Penning trap mass scan frequency range is set to select atomic fission products. The slightly heavier molecular ions remain unobserved. However, they are also selected with the dipole magnet, collected in the RFQ and sent to the Penning trap. If the molecular ions are numerous enough, they can have a similar impact on the trap efficiency as stable bromine beams.

The upper panel in figure 5 shows the time of flight of ions from the Penning trap to the MCP for $A = 88$ and $A = 89$, respectively. The TOF peaks corresponding to masses $A = 88$ and $A = 89$ are at $\approx$180 μs. For $A = 88$ basically only $A = 88$ ions are seen in the TOF spectrum. In the $A = 89$ TOF spectrum a significant amount of other ions with a time of flight of $\approx$100 μs are observed. The mass spectrum corresponding to this 100 μs time of flight peak is flat, showing that these ions are leaking out of the Penning trap independent of the trap frequency. The presence of these ions is an indication that the conditions in the Penning trap are different for $A = 89$ than for $A = 88$.

The IGISOL-4 fission yields for krypton in table 5 have been deduced repeating a similar interpolation as shown in figure 5 for $A = 88$,89 for isobaric chains $A = 87$ - 91. The isotopic yield distribution deduced this way is in agreement with the IGISOL-3 measurements.

Zirconium and molybdenum

No stable background yttrium beam has been observed at IGISOL. As another non-volatile element, zirconium is ex-

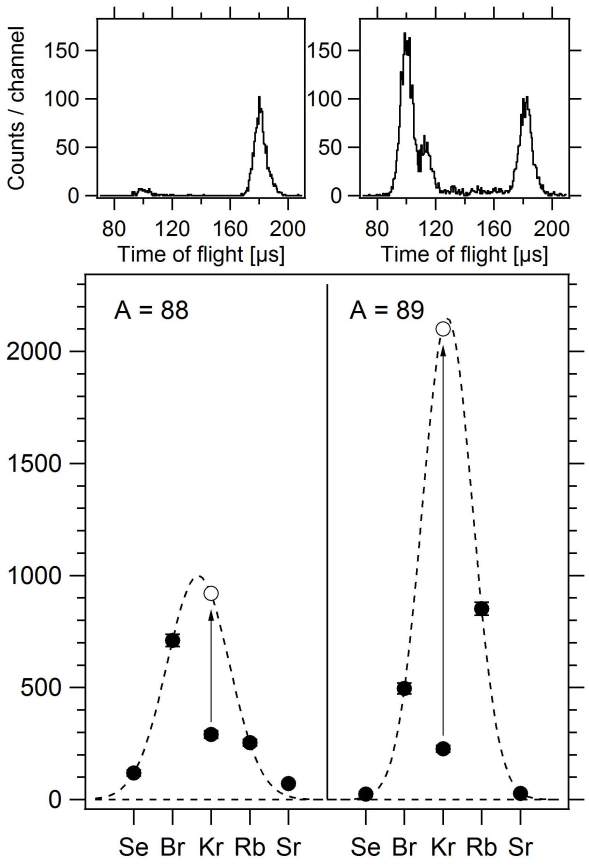

Fig. 5. The isobaric yield distribution for $A = 88$ and $A = 89$. A larger fraction of ^{89}Kr is neutralised than ^{88}Kr. The upper panel shows the time of flight of ions from the Penning trap to the MCP. The TOF peaks corresponding to masses A= 88 and A= 89 are located at ≈180 μs. In mass A = 88 barely any other ions come out of the trap. In A = 89 a significant amount of other ions are observed as indicated by the peak at ≈100 μs.

pected to behave in the same way. The yield of stable ^{96}Zr is 44.7±6.3 %, while its fission yield extrapolated from the radioactive Zr isotopes is 38.3±8.0. This is consistent with all the ^{96}Zr coming directly from fission and supports the assumption that stable zirconium is not present.

The stable molybdenum isotopes ^{96,97,98,100}Mo have abundances 16.7, 9.6, 24.1, and 9.3%, respectively. The fission yield distribution fitted to the radioactive molybdenum isotopes shows that there are more ^{98,100}Mo than expected from fission. The observed intensities of the stable molybdenum beams do not however follow the expected abundances; the intensity of ^{96,97}Mo is significantly less. More precisely, if ^{100}Mo is fixed to an abundance of 9.3%, the observed abundances of ^{96,97,98}Mo are 0.4, 0.3 and 10.6 % (instead of 16.7, 9.6 and 24.1). This underlines the fact that the ionisation mechanism of the stable background isotopes is not properly understood, and the subtraction of their contribution that was successfully performed for ^{76}Ge and ^{82}Se is not necessarily applicable for all elements.

Table 3. Independent isotopic yields in 25 MeV proton-induced fission of ^{nat}U. Value in column "Yield" combines all available measurements. Yields are normalised in such a way that the height of the Gaussian fit to the yields equals 100. Values given in square brackets are interpolations from these fits. Interpolations are given for missing or suspicious values. The uncertainty of the yield is given with a single significant figure precision, when the most significant digit of the uncertainty is 3 or more, and with two significant figures, when it is less than three. All other uncertainties in the table are given to two significant figures.

Isotope	Yield	IGISOL3 yield	IGISOL4 yield
^{74}Zn	62 ± 5		62.2 ± 5.0
^{75}Zn *)	[93]		(69.6 ± 5.4)
^{76}Zn	94.0		94.0
^{77}Zn	44 ± 4		43.9 ± 3.5
^{78}Zn	23 ± 6		23.2 ± 5.4
^{79}Zn *)	[2.7]		^{Br})
^{80}Zn	1.3 ± 1.3		1.3 ± 1.3
^{74}Ga	3.1 ± 0.9		3.08 ± 0.82
^{75}Ga	16.4 ± 1.9		16.4 ± 1.9
^{76}Ga	39		39.0
^{77}Ga	79 ± 4		78.5 ± 3.5
^{78}Ga	107 ± 7		106.8 ± 6.3
^{79}Ga *)	[78.2]		^{Br})
^{80}Ga	42 ± 7		42.2 ± 6.5
^{81}Ga *)	[12.8]		^{Br})
^{82}Ga	1.5 ± 1.1		1.5 ± 1.1
^{74}Ge †,*)	(5.5 ± 0.6) ^{a})		(5.42 ± 0.52)
^{75}Ge	0.13 ± 0.08		0.126 ± 0.078
^{76}Ge †,*)	2.6 ± 0.3 ^{b})		3.7
^{77}Ge	8.7 ± 0.6	8.8 ± 2.2	8.60 ± 0.53
^{78}Ge	35.6 ± 2.2	37.3 ± 9.9	35.0 ± 1.8
^{79}Ge *)	[71.3]		^{Br})
^{80}Ge	98.6 ± 1.7	97.2	96.6 ± 3.9
^{81}Ge *)	[86.3]		^{Br})
^{82}Ge	46.9 ± 3.0	49.0 ± 8.8	45.9 ± 2.7
^{83}Ge	16.4 ± 1.6	15.9 ± 3.9	16.2 ± 1.7
^{84}Ge	4.7 ± 1.6	4.7 ± 1.6	

†) Stable isotope.
*) Excluded from Gaussian fit of the yield distribution.
^{Br}) Yield not measurable due to intense stable bromine background, see text.
^{a}) Stable background. Value is used to estimate background contribution to ^{76}Ge
^{b}) Contribution of background ^{76}Ge estimated from ^{74}Ge and subtracted.

The experimental yields for stable molybdenum isotopes are given in parenthesis in table 7. No attempt was made to subtract the stable background contribution. Instead, the interpolated yield values from a fit to the radioactive isotopes are given in square brackets.

Table 4. Normalised independent isotopic yields in 25 MeV proton-induced fission of ^{nat}U (cont.).

Isotope	Yield	IGISOL3 yield	IGISOL4 yield
^{78}As	1.57		1.57
^{79}As *)	[5.9]		^{Br})
^{80}As	23.8 ± 1.6		23.8 ± 1.6
^{81}As *)	[58.4]		(^{Br})
^{82}As	82 ± 4		82.2 ± 3.4
^{83}As	100.6 ± 2.7		100.6 ± 2.7
^{84}As	66 ± 4		65.6 ± 3.2
^{85}As	21.0 ± 1.9		21.0 ± 1.9
^{86}As	5.6 ± 1.3		5.6 ± 1.3
^{80}Se †,*)	-	98.4 ^{c})	
^{81}Se *)	[58.4]		(^{Br})
^{82}Se †)	29 ± 9	28.8 ± 8.8 ^{d})	^{e})
^{83}Se	65 ± 6	73 ± 14	63.7 ± 5.6
^{84}Se	104 ± 5	175 ± 42	103.8 ± 3.2
^{85}Se	92 ± 4	100.7 ± 5.8	90.6 ± 2.3
^{86}Se	65.7 ± 2.8	68.0 ± 5.0	65.5 ± 2.3
^{87}Se	30.1 ± 1.6	28.9 ± 2.0	31.2 ± 1.7
^{88}Se	11.1 ± 0.9	11.1 ± 0.75	11.2 ± 1.7
^{89}Se	2.2 ± 1.4		2.2 ± 1.4)
^{83}Br	3.7 ± 0.5		3.74 ± 0.44
^{84}Br	18.9 ± 0.4	26 ± 12	19.1
^{85}Br	54.2 ± 1.7	64.6 ± 4.8	53.9 ± 1.5
^{86}Br	79.2 ± 2.6	89 ± 13	79.8 ± 2.3
^{87}Br	99 ± 4	96 ± 13	100.9 ± 2.9
^{88}Br	74 ± 4	87.1 ± 9.1	72.9 ± 3.5
^{89}Br	51.3 ± 2.1	52.55 ± 0.61	50.8 ± 3.5
^{90}Br	17.2 ± 2.0	25.4 ± 4.2	15.2 ± 2.3
^{91}Br	9.4 ± 1.5	9.6 ± 1.6	
^{92}Br	2.2 ± 2.2	2.3 ± 2.3	

†) Stable isotope.
*) Excluded from Gaussian fit of the yield distribution.
^{Br}) Yield not measurable due to intense stable bromine background, see text.
^{c}) Stable background. Value is used to estimate background contribution to ^{82}Se
^{d}) Contribution of background ^{82}Se estimated from ^{80}Se and subtracted.
^{e}) Contribution of background ^{82}Se cannot be subtracted since yield of ^{80}Se is not known.

Table 5. Normalised independent isotopic yields in 25 MeV proton-induced fission of ^{nat}U (cont.).

Isotope	Yield	IGISOL3 yield	IGISOL4 yield
^{87}Kr	32.7 ± 3.0	52.5 ± 6.7	29.3 ± 3.3
^{88}Kr	59 ± 6		60.2 ± 5.3
^{89}Kr	98 ± 5	99.4	99.6 ± 9.4
^{90}Kr	106 ± 9	129 ± 14	97 ± 11
^{91}Kr	59.0 ± 1.6	65.4 ± 5.8	59.6 ± 1.6
^{92}Kr	26.2 ± 2.8	26 ± 4	
^{88}Rb	7.0 ± 0.4		100
^{89}Rb	22.7 ± 0.3	24.2	336 ± 17
^{90}Rb	56.9 ± 3.1	63.8 ± 6.6	802 ± 33
^{91}Rb	99 ± 8	105.7 ± 7.7	
^{92}Rb	84 ± 7	89.7 ± 6.5	
^{93}Rb	89 ± 10	95.0 ± 9.9	
^{94}Rb	41 ± 7	43.5 ± 6.8	
^{95}Rb	30 ± 4	32.2 ± 4.1	
^{96}Rb	13.3 ± 2.0	14.2 ± 2.2	
^{97}Rb	2.6 ± 1.2	2.8 ± 1.3	
^{93}Sr	85 ± 23	85 ± 23	
^{94}Sr	111 ± 17	111 ± 17	
^{95}Sr	98 ± 13	98 ± 13	
^{96}Sr	65.5	65.5	
^{97}Sr	40 ± 5	40.5 ± 4.6	
^{98}Sr	19.6 ± 1.8	19.6 ± 1.8	
^{99}Sr	3.1 ± 0.7	3.08 ± 0.65	
^{100}Sr *)	1.2 ^{u})	1.2 ^{u})	
^{94}Y	41 ± 5	41.4 ± 4.4	
^{95}Y	70 ± 9	69.8 ± 9.0	
^{96}Y	91.1	91.1	
^{97}Y	103 ± 11	103 ± 11	
^{98}Y	94 ± 9	93.8 ± 8.4	
^{99}Y	63 ± 6	62.7 ± 5.3	
^{100}Y	28 ± 4	28.3 ± 3.4	
^{101}Y	9.4 ± 1.1	9.4 ± 1.1	

*) Excluded from Gaussian fit of the yield distribution.
^{u}) Upper limit.

Technetium and ruthenium

For the yields of technetium and ruthenium the same A = 109 reference spectra were used.

The observed yield of ^{106}Tc is much lower than expected. So far unexplained difficulties have been encountered in the precision mass measurements at A = 106 at JYFLTRAP, one possible explanation being an unknown isomer in ^{106}Tc with a half-life of about half a second. This could also explain the low yield of ^{106}Tc in the current experiments, however, such an isomer has not been found so far.

^{106}Ru, on the other hand, shows excess yield. The mass difference between ^{106}Ru and ^{106}Rh is so small that their mass peaks cannot be resolved. The estimated Rh contribution in the mass peak is however too small to explain the excess yield. The whole A = 106 case requires a remeasurement.

No attempt was made to subtract the possible stable background contribution of ^{104}Ru from the yield. Instead, the experimental yield is shown in parenthesis and the extrapolated fission product yield in square brackets.

Table 6. Normalised independent isotopic yields in 25 MeV proton-induced fission of ^{nat}U (cont.).

Isotope	Yield	IGISOL3 yield	IGISOL4 yield
^{96}Zr †,*)	45 ± 7	44.7 ± 6.3 ^{f})	
^{97}Zr	66 ± 11	66 ± 11	
^{98}Zr	111 ± 22	111 ± 22	
^{99}Zr ^{W})	93 ± 11	93 ± 11	
^{100}Zr	82 ± 16	82 ± 16	
^{101}Zr	49.0	49.0	
^{102}Zr	24 ± 6	23.5 ± 5.7	
^{103}Zr	7.2 ± 1.4	7.2 ± 1.4	
^{104}Zr	2.3 ± 0.5	2.32 ± 0.45	
^{105}Zr *)	0.57 ± 0.14	0.57 ± 0.14	
^{97}Nb	1.5 ± 1.5	1.5 ± 1.5	
^{98}Nb	10 ± 9	10.3 ± 8.7	
^{99}Nb ^{W})	35 ± 4	34.7 ± 4.0	
^{100}Nb	52 ± 10	52 ± 10	
^{101}Nb	90.4	90.4	
^{102}Nb	81 ± 20	81 ± 20	
^{103}Nb	77 ± 14	77 ± 14	
^{104}Nb	38 ± 8	38.1 ± 7.9	
^{105}Nb	24.7 ± 1.7	24.7 ± 1.7	
^{106}Nb ^{W})	5.7 ± 0.6	5.72 ± 0.58	
^{107}Nb	2.3 ± 2.4	2.3 ± 2.4	

†) Stable isotope.
*) Excluded from Gaussian fit of the yield distribution.
^{W}) Weighted average.
^{f}) Possible contribution from stable background is not subtracted from the yield.

Cadmium

The yields of $^{115-122}$Cd were determined against ^{119}Cd, and the yields of $^{120-127}$Cd against ^{123}Cd. The $A = 119$ mass spectra were used as a reference also for palladium and silver, while $A = 123$ mass spectra were used as a reference for indium, tin and antimony. The distributions were combined using a similar normalization than for e.g. Ag, Rh, Pd or Br. Unlike in all other cases, the two distributions are in poor agreement with each other (table 2). The widths and centroids of the ^{119}Cd and ^{123}Cd sets disagree. The Gaussian fit to ^{123}Cd set is sensitive to the weighting, since all the yields are on the same side of the distribution centroid. This does however not explain the discrepancies between the ^{119}Cd and ^{123}Cd sets. A systematic, mass-dependent error could in principle explain the observed differences, but the same effects should be seen for indium isotopes, for which ^{123}In was used as the reference isotope. This is not the case.

A further analysis of yield distributions shows that the ^{119}Cd set is in better agreement with the yield distributions of neighboring elements. The yields for Cd were eventually combined by using the ^{119}Cd set for $^{115-122}$Cd and the yields against ^{123}Cd for $^{123-127}$Cd. The distributions were linked at ^{122}Cd and the yields of ^{120,121}Cd against

Table 7. Normalised independent isotopic yields in 25 MeV proton-induced fission of ^{nat}U (cont.).

Isotope	Yield	IGISOL3 yield	IGISOL4 yield
^{97}Mo †,*)	[0.03]	(0.17 ± 0.18) ^{g})	
^{98}Mo †,*)	[0.2]	(5.9 ± 1.1) ^{g})	
^{99}Mo ^{W})	1.78 ± 0.23	1.78 ± 0.23	
^{100}Mo †,*)	[5.8]	(12.3 ± 2.4) ^{g})	
^{101}Mo	18.5	18.5	
^{102}Mo	53 ± 13	53 ± 13	
^{103}Mo	80 ± 15	80 ± 15	
^{104}Mo	106 ± 16	106 ± 16	
^{105}Mo ^{W})	95 ± 6	94.7 ± 5.8	
^{106}Mo ^{W})	78 ± 9	77.6 ± 8.1	
^{107}Mo	27 ± 10	27.0 ± 9.7	
^{108}Mo	7.8 ± 1.4	7.8 ± 1.4	
^{109}Mo	4.2 ± 0.9	4.16 ± 0.89	
^{110}Mo	0.58 ± 0.12	0.58 ± 0.12	
^{101}Tc	0.53 ± 0.16	0.53 ± 0.16	
^{102}Tc	2.3 ± 0.7	2.30 ± 0.64	
^{103}Tc	8.1 ± 1.1	8.1 ± 1.1	
^{104}Tc	19.0 ± 2.1	19.0 ± 2.1	
^{105}Tc	52 ± 6	51.8 ± 5.9	
^{106}Tc *)	[84.3]	(30.0 ± 4.2) ^{h})	
^{107}Tc	104 ± 9	103.7 ± 8.9	
^{108}Tc	74 ± 5	74.2 ± 5.0	
^{109}Tc	53.4	53.4	
^{110}Tc	18.1 ± 1.7	18.1 ± 1.7	
^{111}Tc	10.1 ± 3.0	10.1 ± 3.0	
^{112}Tc *)	2.9 ^{u})	2.9 ^{u})	
^{104}Ru †,*)	[0.8]	(2.26 ± 0.70)	
^{105}Ru	3.6 ± 0.9	3.60 ± 0.85	
^{106}Ru *)	[13.5]	25 ^{u,i})	
^{107}Ru	32.0 ± 2.9	32.0 ± 2.9	
^{108}Ru	67 ± 5	67.4 ± 4.2	
^{109}Ru	94.8	94.8	
^{110}Ru	89 ± 6	88.5 ± 5.2	
^{111}Ru	69 ± 7	69.0 ± 6.7	
^{112}Ru	42 ± 3	42.0 ± 3.0	
^{113}Ru	16 ± 5	16.5 ± 4.3	
^{114}Ru	6 ± 4	5.9 ± 3.2	
^{115}Ru*)	0.5 ^{u})	0.5 ^{u})	

†) Stable isotope.
*) Excluded from Gaussian fits of the yield distribution.
^{u}) Upper limit.
^{W}) Weighted average.
^{g}) Possible contribution from stable background is not subtracted from the yield.
^{h}) The observed yield of ^{106}Tc is likely in error. See text.
^{i}) The observed yield of ^{106}Ru is likely in error. See text.

Table 8. Normalised independent isotopic yields in 25 MeV proton-induced fission of ^{nat}U (cont.).

Isotope	Yield	IGISOL3 yield	IGISOL4 yield
^{105}Rh *)	0.53 ^{u})	0.53 ^{u})	
^{106}Rh *)	[0.2]		
^{107}Rh	1.8 ± 0.8	1.82 ± 0.75	
^{108}Rh	3.5 ± 2.3	3.5 ± 2.3	
^{109}Rh	18.3 ± 1.1	18.3 ± 1.1	
^{110}Rh	43 ± 5	42.7 ± 4.8	
^{111}Rh	97 ± 14	97 ± 14	
^{112}Rh	104 ± 10	104.1 ± 9.7	
^{113}Rh	94 ± 9	94.3 ± 9.0	
^{114}Rh	54 ± 6	54.0 ± 5.2	
^{115}Rh	30.7 ± 2.6	30.7 ± 2.6	
^{116}Rh	15 ± 4	14.6 ± 3.6	
^{109}Pd	0.9 ± 0.6	0.87 ± 0.57	
^{110}Pd †)	5.9 ± 1.4	5.9 ± 1.4	
^{111}Pd	15.8 ± 2.2	15.8 ± 2.2	
^{112}Pd	41 ± 8	41.5 ± 7.9	
^{113}Pd	73 ± 12	73 ± 12	
^{114}Pd	95 ± 8	95.3 ± 7.6	
^{115}Pd	99.5	99.5	
^{116}Pd	91 ± 10	90.5 ± 9.6	
^{117}Pd	53 ± 5	52.9 ± 4.5	
^{118}Pd	28 ± 4	28.4 ± 3.2	
^{119}Pd *)	8.2 ^{u})	8.2 ^{u})	
^{113}Ag	4.4 ± 1.0	4.38 ± 0.98	
^{114}Ag	9.1 ± 2.1	9.1 ± 2.1	
^{115}Ag	34.5 ± 1.9	34.5 ± 1.9	
^{116}Ag	67 ± 7	67.0 ± 6.3	
^{117}Ag	97 ± 9	96.6 ± 8.2	
^{118}Ag	102 ± 10	101.5 ± 9.1	
^{119}Ag	70.0 ± 2.3	70.0 ± 2.3	
^{120}Ag	52 ± 7	52.2 ± 6.3	
^{121}Ag	14.6 ± 1.8	14.6 ± 1.8	
^{122}Ag	3.6 ± 0.9	3.64 ± 0.85	

†) Stable isotope.
*) Excluded from Gaussian fit of the yield distribution.
^{u}) Upper limit.
^{g}) Possible contribution from stable background is not subtracted from the yield.

^{123}Cd rejected from the final analysis. New measurements are needed to confirm the Cd yield distribution.

Indium, tin and antimony

The yields of indium, tin and antimony were extracted from the same mass spectra. The reference mass $A = 123$ was close to optimal for indium and chosen such that the yields of cadmium and tin could also be extracted against the same reference. From this point, the experiments at IGISOL-3 were not continued towards heavier elements because of contamination from stable xenon isotopes. The

Table 9. Normalised independent isotopic yields in 25 MeV proton-induced fission of ^{nat}U (cont.).

Isotope	Yield	IGISOL3 yield	IGISOL4 yield
^{115}Cd	1.8 ± 0.7	1.79 ± 0.70	
^{116}Cd †,*)	[7.1]	(35.7 ± 3.2) ^{j})	
^{117}Cd	19.7 ± 1.0	19.7 ± 0.92	
^{118}Cd	50.5 ± 1.6	50.5 ± 1.6	
^{119}Cd	77.7	77.7	
^{120}Cd	92 ± 3	91.6 ± 2.7	
^{121}Cd	78 ± 7	78.1 ± 6.3	
^{122}Cd *)	45.4 ± 1.2	45.4 ± 1.2	
^{123}Cd	43.0 ± 2.5	43.0 ± 2.5	
^{124}Cd	21 ± 4	20.8 ± 3.6	
^{125}Cd	11.7 ± 1.8	11.7 ± 1.8	
^{126}Cd	3.1 ± 1.1	3.1 ± 1.1	
^{127}Cd	1.5 ± 0.8	1.46 ± 0.77	
^{117}In	0.49 ± 0.29	0.47 ± 0.29	
^{118}In	[1.8]		
^{119}In	6.7 ± 1.3	6.4 ± 1.3	
^{120}In	19.2 ± 1.7	18.4 ± 1.7	
^{121}In	44.1 ± 3.0	42.2 ± 2.9	
^{122}In	76 ± 12	73 ± 12	
^{123}In	103 ± 4	96.8	102.7 ± 4.9
^{124}In	89 ± 6	97.8 ± 8.7	82.1 ± 6.1
^{125}In	68 ± 6	66.8 ± 6.8	64.5 ± 7.4
^{126}In	44 ± 4	44.6 ± 5.1	42.4 ± 3.7
^{127}In	[17.7]		^{I})
^{128}In	7.4 ± 0.3		7.30
^{129}In	2.0 ± 0.4	2.0 ± 0.4	1.96 ± 0.40
^{120}Sn †,*)	[0.5]	(1.04 ± 0.14)	
^{121}Sn	2.4 ± 0.5	2.40 ± 0.45	
^{122}Sn †,*)	[8.0]	(9.26 ± 0.93)	
^{123}Sn	22.0 ± 0.3	23.2	20.1 ± 2.4
^{124}Sn †,*)	[47.6]	(74.6 ± 6.1)	(104.6± 1.3) ^{j})
^{125}Sn	91 ± 4	74 ± 14	94 ± 21
^{126}Sn	99 ± 14	100 ± 14	^{NR})
^{127}Sn	100 ± 13	101 ± 13	^{I})
^{128}Sn	71 ± 4	66 ± 13	73.3 ± 1.9
^{129}Sn	37.9 ± 2.2	^{Xe})	38.75 ± 0.78
^{130}Sn	20.8 ± 0.9	15.3 ± 4.4	21.5 ± 1.2
^{131}Sn	9.30 ± 0.21	^{Xe})	9.50 ± 0.37
^{132}Sn	3.06 ± 0.23	^{Xe})	3.13 ± 0.25
^{133}Sn	1.01 ± 0.14	1.02 ± 0.14	

†) Stable isotope.
*) Excluded from Gaussian fit of the yield distribution.
^{Xe}) Yield not measurable due to intense stable xenon background, see text.
^{I}) Yield not measurable due to intense stable iodine background, see text.
^{NR}) Not resolvable.
^{j}) Possible contribution from stable background is not subtracted since background cannot be estimated.

Table 10. Normalised independent isotopic yields in 25 MeV proton-induced fission of ^{nat}U (cont.).

Isotope	Yield	IGISOL3 yield	IGISOL4 yield
^{123}In		34 [i]	
^{126}Sb	23 ± 13	24 ± 13	
^{127}Sb	52 ± 5	55.6 ± 4.5	[I]
^{128}Sb	71 ± 5	82.6 ± 8.6	74.3 ± 4.7
^{129}Sb [*]	[98.4]	[Xe]	(122.8 ± 8.7) [j]
^{130}Sb	89 ± 4	88 ± 10	94.7 ± 2.6
^{131}Sb	67.7 ± 1.8	[Xe]	71.8
^{132}Sb	34.7 ± 1.7	[Xe]	36.8 ± 1.5
^{133}Sb [k]	12.0 ± 0.6	8.53 ± 0.82	14.36 ± 0.58
^{134}Sb	2.8 ± 1.2		3.0 ± 1.2
^{135}Sb	0.88 ± 0.12		0.94 ± 0.13
^{129}Te	67.8 ± 1.7		67.8 ± 1.7
^{130}Te [†]	[89.9]		[l]
^{131}Te	99.8		99.8
^{132}Te	[104.1]		[NR]
^{133}Te	92.8 ± 2.8		92.8 ± 2.8
^{134}Te	61 ± 12		61 ± 12
^{135}Te	22.2 ± 0.6		22.25 ± 0.62
^{136}Te	13.7 ± 0.5		13.71 ± 0.45
^{137}Te	6.2 ± 0.4		6.17 ± 0.37
^{131}I	19.9 ± 1.8		19.9 ± 1.8
^{132}I	51.2 ± 0.8		51.82 ± 0.74
^{133}Te			[i]
^{133}I	[76.7]		[NR]
^{134}I	99.7 ± 1.3		99.7 ± 1.3
^{135}I	[90.6]		[NR]
^{136}I	65.9 ± 1.0		65.93 ± 0.92
^{137}I	50.3 ± 6.5		50.3 ± 6.5
^{138}I	19.2 ± 2.7		19.2 ± 2.7
^{139}I	7.7 ± 1.4		7.7 ± 1.4

[†]) Stable isotope.
[*]) Excluded from Gaussian fits of the yield distribution.
[Xe]) Yield not measurable due to intense stable xenon background, see text.
[I]) Yield not measurable due to intense stable iodine background, see text.
[NR]) Not resolvable.
[i]) Used as a reference isotope. Yield value as such has no meaning.
[j]) Sum of ^{129}Sb (53%) and ^{129m}Sb (47%), see text.
[k]) Uncertainty estimated from the difference of IGISOL-3 and IGISOL-4 measurements.
[l]) Saturated yield.

Table 11. Normalised independent isotopic yields in 25 MeV proton-induced fission of ^{nat}U (cont.).

Isotope	Yield	IGISOL3 yield	IGISOL4 yield
^{137}Xe		84 ± 20	106.5 ± 2.9
^{138}Xe		55 ± 13	78.6 ± 2.4
^{139}Xe		16 ± 3	60.1 ± 1.8
^{140}Xe		7.0 ± 1.4	32.66 ± 0.87
^{141}Xe		1.4	8.73 ± 0.33
^{142}Xe		0.4 ± 0.2	2.41 ± 0.22
^{138}Cs	87.6 ± 3.0	94.3 ± 9.4	88.08 ± 0.86
^{139}Cs	95 ± 4	91 ± 11	96.56 ± 0.87
^{140}Cs	84.3 ± 2.9	77 ± 12	85.6
^{141}Cs	65.2 ± 2.1	59	68.75 ± 0.75
^{142}Cs [*]	32.8 ± 1.3	29.4 ± 3.1	33.65 ± 0.71
^{143}Cs	12.3 ± 1.6	12.4 ± 1.3	
^{144}Cs	2.5 ± 0.5	2.54 ± 0.46	
^{145}Cs	0.64 ± 0.25	0.64 ± 0.25	
^{138}Ba [†,*])	[22.6]	38 [u])	
^{139}Ba	44 ± 6	44.2 ± 5.5	
^{140}Ba	79 ± 12	79 ± 12	
^{141}Ba	100	100.2	
^{142}Ba	76 ± 8	76.3 ± 7.9	
^{143}Ba	58 ± 6	57.7 ± 6.0	
^{144}Ba	30 ± 5	29.7 ± 4.7	
^{145}Ba	8.1 ± 0.9	8.11 ± 0.90	
^{146}Ba	3.5 ± 0.4	3.47 ± 0.42	
^{147}Ba	0.69 ± 0.29	0.69 ± 0.29	
^{148}Ba [*])	0.14 [u])	0.14 [u])	
^{139}La [†,*])	4.9 [u])	4.16[u])	
^{140}Xe			121 [i])
^{140}La	[15.1]		
^{141}La	44	37.1	37.1 ± 0.83
^{142}La	72.7 ± 2.1	(44 ± 14)	57.1 ± 1.7
^{143}La	133 ± 34	113 ± 29	
^{144}La	131 ± 32	111 ± 28	
^{145}La	77 ± 12	66 ± 10	
^{146}La	42 ± 6	35.3 ± 4.5	
^{147}La	17.5 ± 2.5	14.9 ± 2.1	
^{148}La	4.6 ± 0.9	3.90 ± 0.75	

[†]) Stable isotope.
[*]) Excluded from Gaussian fit of the yield distribution.
[u]) Upper limit.
[i]) Used as a reference isotope. Yield value as such has no meaning.

most abundant xenon isotopes prevented measurements in mass numbers A = 129,131 and 132. The less abundant allowed proper measurements only further from stability. The yield of antimony was therefore not measured against an appropriate reference isotope. However, the frequency range of the collected mass spectra in the $A = 123$ reference set covered also antimony mass peaks for $A \geq 126$. Practically no ^{123}Sb is produced in fission, which itself is a stable isotope. The yield of antimony isotopes were determined against ^{123}In instead. Since the ratio of ^{123}Sn to ^{123}In remained constant throughout the measurement, it is reasonable to assume that conditions stayed stable for antimony as well.

The IGISOL-4 measurements were in general more precise than those at IGISOL-3. This is particularly true for tin and antimony. The IGISOL-4 independent yields for

antimony agree for the most part with IGISOL-3, which further supports the use of an indium reference isotope for antimony. The ^{133}Sb yield is however in disagreement. For the final yield of ^{133}Sb, a weighted average is adopted, as usual. The uncertainty is calculated from the difference of the two disagreeing values.

The vast majority of In, Sn and Sb nuclei is known to have isomeric states. Of the studied isotopes only ^{126,133}Sn and ^{127,133}Sb do not have a long-lived isomer. In addition, these states are irresolvable with the mass resolving power in these experiments. This increases the uncertainty of the decay loss corrections, in particular when the isomers have very different half-lives and the isomeric ratio is not known. In [42] the isomeric ratios for 30 isomers were determined in 24 MeV proton-induced fission of ^{238}U. These values were utilised whenever possible. If nothing else was known, an equal production of isomeric states was assumed. The difference of the decay loss corrections for the isomers was used to estimate the uncertainty of the applied correction.

In particular, ^{123}In used as a reference isotope has two isomers with different half-lives (6.17 s and 47.4 s). Their isomeric ratio is not known. An equal population of isomers in fission was assumed. The upper limit of the decay loss correction uncertainty was estimated to be ± 3 %. This uncertainty was not added to the calculated yield ratios. Instead, after the final normalisation of the independent yield distribution of indium, a 3 % uncertainty was added to the ^{123}In normalised yield.

The mass difference between ^{129}Sb and ^{129m}Sb is so large that the mass peaks can be resolved from the A = 129 spectrum. The decay corrections can be applied independently to each isomeric state. The combined yield seems however to be 15% higher than expected.

Tellurium and iodine

Due to the presence of natural xenon isotopes, only the yield ratio of ^{138}I and ^{139}I could be determined at IGISOL-3. This result agrees with the IGISOL-4 measurement.

At IGISOL-4, use of xenon as a calibration gas has been intentionally avoided. Although there is still a small amount of xenon as an impurity in the helium, all mass numbers could be measured. The challenge of properly resolving the densely packed mass peaks however remained, and not all mass peaks were resolvable.

A few tellurium isotopes have isomers separated by 1 - 2 Hz. This makes fitting peaks difficult, since the isomers broaden and skew the tellurium mass peak, so that its width cannot be fixed in the fit. Most of the tellurium mass peaks could be resolved without a fit, even though the peak tails were overlapping with antimony and iodine. ^{134}Te with no known isomers could be resolved from ^{134}I by a fit, while ^{132}Te remained unresolved.

Tellurium is the lightest isotope for which the auxiliary data from IGISOL-4 yield measurement preparation can be utilised. The yields for $^{135-137}$Te agree with the properly measured values. It has to be noted that while data are lacking for ^{128,130,132}Te, the fit is very sensitive to the yield of ^{129}Te.

Resolving the iodine mass peaks was even more challenging than tellurium. ^{133,135}I could not be reliably resolved, the major problem being that A=133 was used as a reference mass. ^{133}Te was used as a secondary reference isotope instead. In addition, since the fitted tellurium yield distribution always lies below the experimental yield of ^{134}Te, it is likely that the ^{134}I yield should be higher. $^{133-135}$I have the highest fission yield of all the iodine isotopes. The yields of ^{133,135}I could not be determined and the ^{134}I yield is suspicious, which adds uncertainty in the distribution parameter fit.

Xenon, cesium, barium and lanthanum

In the IGISOL-3 measurements the yields for elements from xenon to lanthanum were deduced against the same A = 141 reference set. The aim was to have a mass spectrum where all four reference peaks were as well separated as possible. In particular, the reference isotope ^{141}Xe is quite far from stability. This results in a large uncertainty close to the maximum of the yield distribution. For barium the reference isotope ^{141}Ba is in the middle of the yield distribution. The main issue for barium isotopes is correcting the yield fluctuations due to the dipole magnet.

Basically no xenon mass peaks could be resolved for A < 137 either at IGISOL-3 or IGISOL-4. At IGISOL-3, resolving the mass peaks of even more neutron-rich xenon isotopes required fitting, while at IGISOL-4 only the tails of the mass peaks were overlapping. Combining the results becomes difficult, since the maximum of the fission yield distribution seems to be below A = 137. Utilising the A = 135 mass spectrum of the auxiliary mass spectra and subtracting the estimated contribution of ^{135}Cs and ^{135}I on the basis of I and Cs yield distributions allowed estimating the yield of ^{135}Xe. The centroid of the Gaussian fit to the yields of ^{135}Xe and $^{138-142}$Xe is $A_p \approx 136.6$.

It was however not possible to scale the xenon yield distributions from IGISOL-3 and IGISOL-4 in such a way that they could have been combined. In table 11 no combined yield for xenon isotopes is thus given.

Similar to xenon, the mass peaks of cesium in A < 138 are irresolvable. At IGISOL-3 there was indication that the yield of ^{137}Cs was higher than that of ^{138}Cs. At IGISOL-4 the ^{137}Cs mass peak could not be properly resolved, but its yield was clearly smaller than that of ^{138,139}Cs. Using the yield of ^{137}Xe as a reference, the yield of ^{138}Cs was determined to be 91 % of the yield of ^{139}Cs, indicating that the maximum of the distribution is close to A = 139. The same ^{138}Cs/^{139}Cs yield ratio was determined also using ^{137}I as a reference. The ^{137}Cs yield value from the IGISOL-3 measurement was rejected and the IGISOL-3 and IGISOL-4 results combined.

In the fit of the cesium yield distribution the yield of ^{141}Cs was excluded. Its independent yield is always about 15 % higher than the fit. The same excess is observed in the 50 MeV proton-induced fission. It is unlikely that this

Table 12. Independent isotopic yields in 50 MeV proton-induced fission of ^{nat}U

Isotope	Yield	Reference 1	Reference 2	**Isotope**	Yield	Reference
^{73}Zn	80 ± 7	79.7(*75.2*) ± 6.6		^{97}Zr	60 ± 7	77.4(*72.7*) ± 8.0
^{74}Zn	100	100		^{98}Zr	128 ± 27	165 ± 34
^{75}Zn	72 ± 8	72.4 ± 7.2		^{99}Zr	123 ± 20	159(*151*)± 25
^{76}Zn	50 ± 6	49.7 ± 5.7		^{100}Zr	77.5	100
^{77}Zn	14 ± 4	14.1 ± 3.3		^{101}Zr	39 ± 5	50.8(*45.9*) ± 5.4
^{78}Zn	5.5 ± 2.1	5.5 ± 2.1		^{102}Zr	22 ± 4	27.8 ± 4.3
				^{103}Zr	5.9 ± 0.8	7.58(*6.82*)± 0.91
^{73}Ga	9.6 ± 1.0	42.9(*41*)± 4.3		^{104}Zr	1.3 ± 0.4	1.69 ± 0.48
^{74}Ga	22.4	100		^{105}Zr	0.7 ^{u})	0.91(*0.84*) ^{u})
^{75}Ga	58 ± 6	260 ± 24				
^{76}Ga	97 ± 10	431 ± 45		^{109}Pd	4.4 ± 1.3	5.5 ± 1.6
^{77}Ga	111 ± 10	497 ± 42		^{110}Pd ^{†,b})	[12] 17.6±2.0	22.1 ± 2.5
^{78}Ga	71 ± 7	319 ± 28		^{111}Pd	30 ± 4	38.0 ± 4.1
^{79}Ga	34.6 ± 2.7	155 ± 12		^{112}Pd ^{c})	[61] 78 ± 5	98.6 ± 5.7
				^{113}Pd	83 ± 9	105 ± 11
^{87}Rb †)	4.4 ± 1.0^{a})		4.5 ± 1.0	^{114}Pd	96 ± 9	121(*117*)± 11
^{88}Rb	18.7 ± 1.0	100	16.1 ± 1.6	^{115}Pd	79.5	100
^{89}Rb	45.4± 1.7	255(*286*) ± 27	45.5 ± 1.8	^{116}Pd	41 ± 6	52.1 ± 6.6
^{90}Rb	74.0 ± 2.0	404 ± 44	74.7 ± 2.0	^{117}Pd	17 ± 4	21.7 ± 4.4
^{91}Rb	98.7 ± 0.3	490 ± 51	100	^{118}Pd	7.1 ± 0.7	8.91 ± 0.82
^{92}Rb	89 ± 5	409(*306*) ± 51	91.1 ± 4.7	^{119}Pd	3.2 ± 0.7	4.07 ± 0.78
^{93}Rb	74.9 ± 2.5	287 ± 30	77.2 ± 2.7	^{120}Pd	1.0 ^{u})	1.2 ^{u})
^{94}Rb	26.1 ± 1.4	145 ± 11	25.4 ± 1.6			
^{95}Rb	8.4 ± 1.0	105 12	6.5 ± 1.1	^{137}Cs *)	[73] (135 ± 54)	226(*214*) ± 90
^{96}Rb	10.7 ± 1.5	53 ± 7		^{138}Cs	102 ± 7	170(*157*) ± 11
				^{139}Cs	95 ± 10	159 ± 16
^{93}Sr	85 ± 23	130 ± 35		^{140}Cs	75 ± 5	125(*115*) ± 7
^{94}Sr	111 ± 17	170(*145*) ± 26		^{141}Cs ^{d})	[54] 59.7	100
^{95}Sr	98 ± 12	149 ± 19		^{142}Cs	31.6 ± 1.7	52.9(*55.6*) ± 2.7
^{96}Sr	65.5	100		^{143}Cs	12.8 ± 1.0	21.5 ± 1.7
^{97}Sr	40 ± 5	61.8 (*64.8*) ± 6.8		^{144}Cs	3.6 ± 0.3	6.12 ± 0.49
^{98}Sr	19.7 ± 1.8	30.0 ± 2.7		^{145}Cs	1.2 ± 0.3	2.04 ± 0.44
^{99}Sr	3.1 ± 0.7	4.7 ± 1.0		^{146}Cs	0.19 ± 0.14	0.31 ± 0.22
^{100}Sr	1.2 ^{u})	1.9(*1.8*) ^{u})				

†) stable isotope
*) Excluded from Gaussian fit of the yield distribution.
^{u}) Upper limit.
^{a}) Stable background contribution to ^{87}Rb subtracted based on measured yield of ^{85}Rb
^{b}) Includes stable background contribution to ^{110}Pd.
^{c}) Includes irresolvable ^{112}Ag contribution.
^{d}) Reference isotope, but excluded from the Gaussian fit, see text.

is a real effect due to nuclear structure. The ^{141}Cs half-life is so long (24.9 s) that the effect cannot come from decay corrections. The centroid of the combined yield distribution becomes 138.94 ± 0.05. The fit is sensitive to the ^{138}Cs yield, determined using ^{137}Xe(^{137}I) as a reference. The centroid can be compared to a linear interpolation of the centroids of neighboring Sb, Ba and La distributions determined in this work, which gives 138.8 ± 0.2. In Tracy *et al.* [43] the fission yield distributions for 40, 50 and 60 MeV proton-induced fission were determined. A linear extrapolation to 25 MeV proton-induced fission results in 138.5 ± 0.2 as a centroid.

The IGISOL-4 measurement extended only up to $A = 142$. Therefore, they did not contribute heavily to the lanthanum yield measurements. However, the ratio ^{141}La/^{142}La = 0.6015 ± 0.0168 was determined. Since ^{141}La was used as a reference isotope in the IGISOL-3 measurements, the value can straightforwardly be applied to adjust the yield of ^{142}La. The IGISOL-4 measurement is so precise that it almost solely determines the ^{142}La yield and increases it by 60%. In fact, the Gaussian fit to the IGISOL-3 yield

distribution strongly suggests that the determined ^{142}La yield is too low.

3.2 50 MeV proton-induced fission

The yield measurement with 50 MeV protons was made for fewer elements than for 25 MeV protons, however covering as many different fission regions as possible: zinc and gallium in the wing of the light mass peak, rubidium, strontium and zirconium in the middle of the light mass peak, palladium in the region of symmetric fission and cesium in the heavy mass peak. Yields of rubidium and cesium were important since they gave a direct comparison to the work of Tracy *et al.* [43] for the verification of the Penning trap-based fission yield measurements [29]. These measurements took place at IGISOL-3.

Rubidium

The rubidium yield distribution was determined with respect to ^{88}Rb and ^{91}Rb. ^{88}Rb as a reference has the disadvantage in that it is at the side of the yield curve, while ^{91}Rb is close to the maximum. The yield curve using ^{91}Rb as a reference has been published in [29] where it was compared to the Rb yields determined by Tracy *et al.* [43]. The agreement between the ^{91}Rb set and reference [43] was excellent up to ^{93}Rb; the determined yield for ^{94,95}Rb fall below the data of Tracy *et al.*. For the ^{88}Rb set, the data agrees with reference [43] up to ^{92}Rb, and now ^{95,96}Rb values are above Tracy *et al.* data. The combined yields are given in table 12.

Palladium

The ^{112}Pd peak is irresolvable from ^{112}Ag. Unlike in the case of 25 MeV proton-induced fission, the contribution of ^{112}Ag could not be estimated on the basis of the isotopic yield curve of silver. The independent yield of ^{112}Pd can thus not be determined. The upper limit including both ^{112}Pd and ^{112}Ag is given in parenthesis, the interpolated yield in square brackets in table 12.

Cesium

Similar to 25 MeV proton-induced fission, the obtained ^{137}Cs yield was exceptionally high. Since this high yield was not seen in the later measurements in 25 MeV fission, it seems likely that the high yield of ^{137}Cs is due to background ions that cannot be distinguished from ^{137}Cs in the mass spectrum. The ^{137}Cs yield is thus not included in the Gaussian fits of cesium isotopic fission yield distribution.

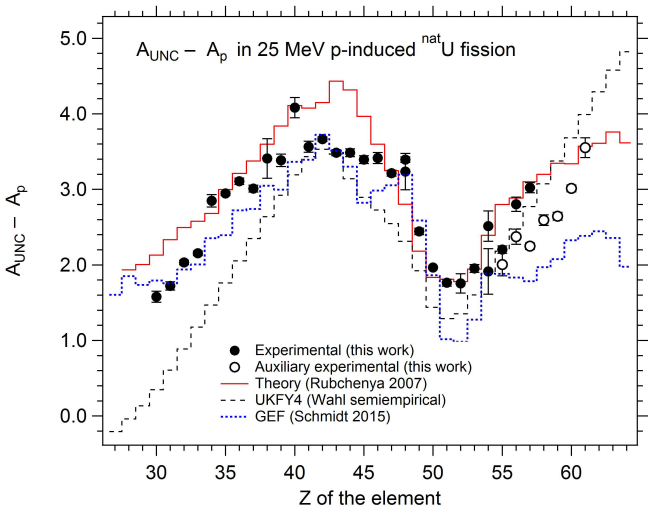

Fig. 6. The difference between the experimental A_p of the isotopic yield distribution and A_{UNC} in 25 MeV proton-induced fission of ^{nat}U (solid symbols). The open symbols represent A_{UNC} - A_p deduced from the auxiliary data described in section 2.2.2. A_{UNC} corresponds to the proton/neutron ratio of the compound nucleus ^{239}Np. The predictions of Rubchenya [44,45] and Wahl [46–48] models are given for comparison (lines).

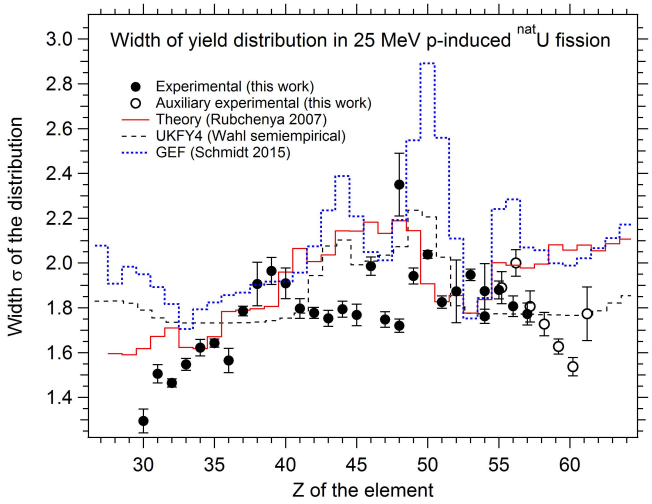

Fig. 7. The widths σ_A of the isotopic yield distributions (solid symbols). The open symbols represent widths deduced from the auxiliary data described in section 2.2.2. The predicted widths from Rubchenya [44,45] and Wahl [46–48] models are given for comparison (lines).

4 Discussion

4.1 Summary of the yield distributions

The experimental results of the independent isotopic fission yield distributions can be summarized with the positions A_p and widths σ_A of the yield distributions for each element. In order to visualise the evolution of A_p it is compared to the unchanged nucleon composition value A_{UNC}, which has the same neutron/proton ratio as the ^{239}Np

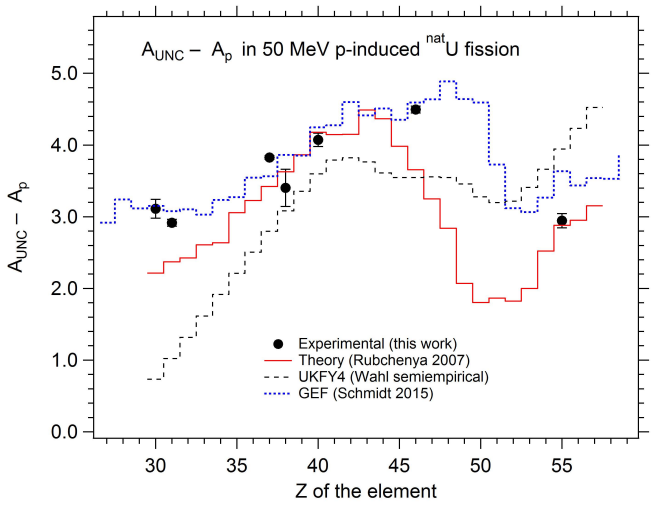

Fig. 8. As figure 6 for 50 MeV proton-induced fission.

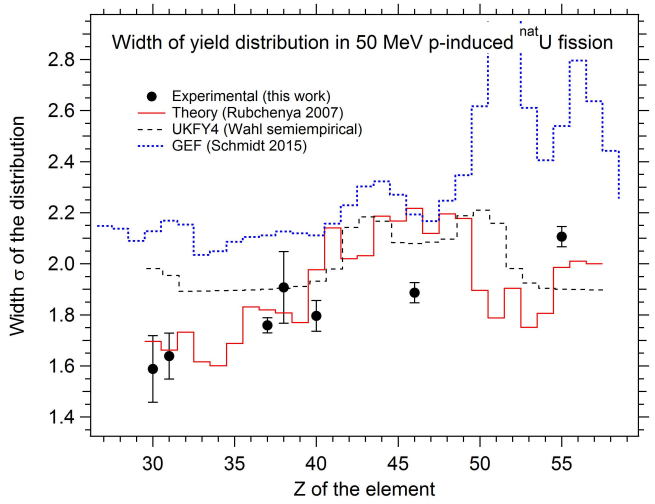

Fig. 9. As figure 7 for 50 MeV proton-induced fission.

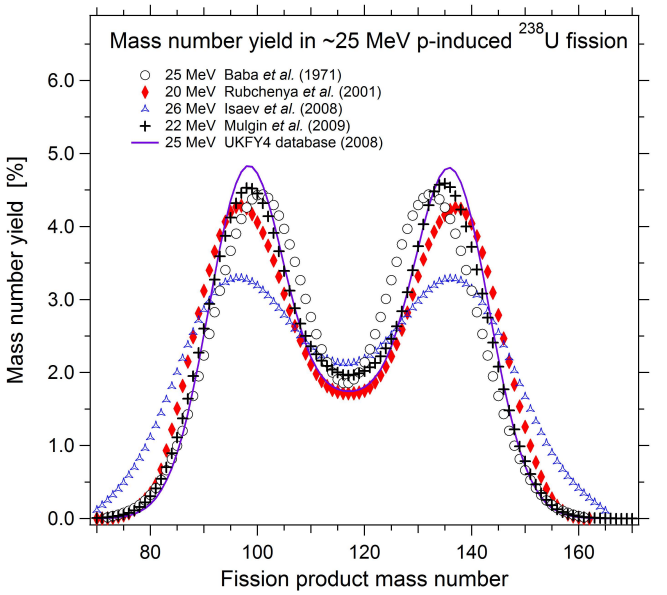

Fig. 10. The mass number yield distributions for ≈ 25 MeV proton-induced fission from references [48,6,7,5,49]. The agreement between the mass yields is poor.

compound nucleus. In our earlier paper [31] A_{UNC} was referred to as A_{UCD}, where UCD stands for unchanged charge distribution. Since there is a UCD model [50], which assumes uniform proton density in the fissioning system during the fission process, but also takes into account the emitted neutrons, the term used here is modified to avoid confusion.

The difference between A_{UNC} and A_p is displayed in figures 6 and 8 for 25 MeV and 50 MeV proton-induced fission, respectively. Two experimental values are given for cadmium and xenon, since the current measurement cannot distinguish between the two deduced possibilities. The distribution width σ_A is shown in figure 7 for 25 MeV and in figure 9 for 50 MeV proton-induced fission.

The difference A_{UNC} - A_p can be interpreted as an average total neutron emission for each element. However, the data cannot distinguish at which stage the neutrons were emitted: during the formation of the compound nucleus, during the decay of the compound nucleus (the excitation energy is sufficient to allow a second change fission after neutron emission), or from the fragment.

As well as the properly measured isotopic yield distributions, the fit results for the auxiliary data measured as described in paragraph 2.2.2 are displayed with open circles. In addition to the experimental results from this work, the difference A_{UNC} - A_p is shown for the Rubchenya fission model [44,45], the General fission (GEF) model [**?**] as well as for the Wahl model [46–48]. Since the main goal of this paper is publishing experimental results, the models are summarised in the following only very briefly.

The Wahl model [46,47] is based on interpolating the systematic trends of the experimentally known fission yield distributions. The available experimental distributions are fitted and the evolution of the fit parameters is studied as a function of the mass number A_c, total charge Z_c and excitation energy E_c^* of the compound nucleus. The independent yields are extracted from two models that give different perspective on the yield distribution: Z_p model, describing the most probable nuclear charge and its dispersion for a given fission fragment mass number, and $A_p^{'}$ model, describing the mass distributions of fission fragments. Fragment distributions are used as the basis of the model instead of product distributions, because the sum of the mass number of the complementary fragments is that of the fissioning system.

Since the yields from the Wahl model are based on the least squares fit of parameters of another fits, the model tends to smooth out the possible fine structure present in the empirical data. This is readily observed in figures 6,8,7,9, where the predicted trends of the isotopic yield distribution location and width are monotonic as compared the more detailed variation of the predictions of the Rubchenya model.

The data used for comparison are taken from the UKFY4 data base [48]. The yields of 25 MeV proton-induced fission of ^{238}U are linearly interpolated from the yields for 20 MeV and 30 MeV proton-induced fission of the data base, while yields of 50 MeV proton-induced fission are taken directly from the data base.

While the Wahl model observes only the final outcome of the fission, the Rubchenya model [45] explores and models all the stages of the process to predict the fission yields. First, the formation of the fissioning compound nucleus is modelled. Neutron and proton emission during the pre-equilibrium stage is described using the two-exciton model and Monte Carlo approach. The mass, charge and excitation energy distributions of the compound nuclei are calculated. Second, the decay of the excited compound nuclei either via the statistical particle emission, gamma emission or fission is modelled. The fission width is considered to be both time and nuclear friction dependent. The primary fission fragment mass yield distributions are calculated using a multimodal approach with five fission modes: symmetric, two asymmetric, and two superasymmetric. The parameters of the fission modes are obtained from fits to the experimental data. Isobaric charge distributions of the primary fragments are considered to be due to quantal fluctuations of the isovector nuclear matter density at the finite scission neck. Finally, the de-excitation process of the heated primary fragments via particle excitation is modelled to obtain the fission product yield distributions.

The GEF model developed by K.H. Schmidt is a general description of fission process. The model is comprehenisvely described in [51] and [52]. The open GEF source code is availailable at [53]. Significant to the GEF model is that it stresses the role of nascent fragments as the source of shell effects in the fission process. Similarly to the Rubchenya model, GEF takes in the account the entire fission process starting from the formation of the compound nucleus (entrance channel), follows the dynamical evolution of the system up to scission utilising statistical mechanics to predict the distribution of energy in the system, and finally considers prompt particle (neutron) emission from the fission fragments, which is needed to predict the fission yields. Moreover, the competition between the particle emission, gamma emission and fission from excited states has been be modelled to be able to consider multichange fission.

The GEF model parameters have been adjusted in a global fit to experimental data. Unlike in Wahl model, the fitted parameters are not direct observables, but physical parameters such as fission barrier heights, nuclear level densities and partial decay widths of nulear states. Approximations and global fits of parameters are favored over microscopic calculations to ensure fast computing and predictions for fissioning systems of which no empirical data are available. The GEF model allows to fine tune its parameters for a better local performance. The calculations shown in this paper are made with GEF version 2015/2.2 [53] using default parametrisation without adjustments.

All models predict the largest difference from A_{UNC} in the region of the symmetric fission, from where the difference is expected to gradually decrease towards both the light nuclei and the region of the heavy mass peak above doubly magic ^{132}Sn. This reflects the view that in symmetric fission the fission fragments are more excited and evaporate more neutrons. This picture is however not fully supported by the experiment. The experimental difference A_{UNC} - A_p is almost constant from Z = 38 (strontium) to Z = 48 (cadmium) before it starts declining towards the heavy mass peak region. Elsewhere the trends predicted by the models are followed. The actual values are closest to the predictions of the GEF model, in particular up to Z = 50. Above Z = 50, Wahl interpolation and Rubchenya model are doing better.

The A_p values deduced from the auxiliary data do not fully agree with the more precisely measured experimental data. The values seem to be systematically smaller, the reason of which is unclear. Nevertheless, it can be concluded from the auxiliary data that the difference A_{UNC} - A_p keeps increasing beyond lanthanum (Z = 57), as predicted by the models.

The experimental widths of the isotopic distribution, as well as the widths predicted by the models, are displayed in figure 7. The models predict wider isotopic yield distributions in the region of symmetric fission, in accordance with higher excitation in symmetric fission. The experimental widths however do not follow the predicted trend but remain more or less constant from Z = 40 to Z = 48. This lower-than-predicted dispersion region interestingly coincides with the "flat" region of A_{UNC} - A_p distribution. While GEF model gives the best prediction for the centroids of the isotopic distributions, the predicted widths are considerably higher than the experimental ones. Therefore, Rubchenya model seems to have the best overall agreement with the data.

The experimental widths deduced from the auxiliary data set (open circles in figure 7) show an interesting tendency of narrower isotopic yield distributions towards the heavier elements. This is clearly against expectations. Since it is based on shortly measured auxiliary datasets, it can be due to some hidden experimental error. Nevertheless, it suggests that at least some clarifying experiments on 25 MeV proton-induced fission yields are still needed in the heavy mass peak.

The obtained data are more sparse for 50 MeV proton-induced fission. GEF model seems to predict the centroids of the isotopic yield distributions most accurately, but yields far too wide distributions, for which the measured yields seem to support the Rubchenya model predictions.

4.2 Absolute independent yields

The independent isotopic yields can be converted to absolute yields, if the mass number yields are known. The mass number yield Y_A for mass number A is

$$Y_A = \sum_Z Y_{A,Z} = \sum_Z k_Z Y^n_{A,Z}. \quad (2)$$

In the equation $Y_{A,Z}$ is the independent yield of an isotope ^{A}Z and $Y^n_{A,Z}$ the normalized independent isotopic

yield (as given in tables 3 to 11). The independent yields can be calculated from the normalised isotopic yields by multiplying by k_Z, a scaling factor for element Z. A mass yield distribution of fission consists of about 100 Y_A values, while there are less than 50 isotopic yield distributions. This gives enough equations to solve the scaling factors k_Z.

4.2.1 Mass number yield

Data on the mass number yields in proton-induced fission is sparse. The mass yields for 25 MeV proton-induced fission of ^{238}U have been experimentally determined in the work of Baba et al. [5]. In addition, mass yields have been determined for 20 MeV proton-induced fission in ref. [7], for 22 MeV proton-induced fission in ref. [49], and for 26 MeV proton-induced fission in ref. [6].

In [5] the cumulative yields of 15 isotopes and the independent yields of four shielded isotopes were determined utilising chemical separation and subsequent $4\pi\beta$- and $4\pi\beta - \gamma$-coincidence counting. The mass yield curves were fitted with three Gaussian distributions. The data and the details of the fit given in [5] are used to reproduce the fission mass yield distribution displayed in figure 10. The data in [5] is so sparse (19 measured mass yields) that the full distribution has to be constructed by a fit. The original approach with three Gaussian distributions is adopted in the present work, since a fit with two asymmetric modes (five Gaussians) does not improve the fit.

In references [7] and [6] the fission products recoiling out of a thin target were observed in a scattering chamber. The fission recoils and their energy were detected using either position sensitive avalanche counters [7] or Multi-Wire Proportional gas Counters (MWPCs) [6]. The mass assignments were based on kinetic energy and time of flight measurements. In [7] the mass yields were deduced for 20, 35, 50 and 60 MeV, in [6] for 26.5 and 61 MeV proton-induced fission of ^{238}U.

In [49] mass yield (and kinetic energy) distributions for 22 MeV proton-induced fission of ^{238}U were determined using a pair of surface-barrier silicon detectors. 2E-technique was applied to a fission product pair observed in coincidence. A strict coincidence gate was used to reduce the number of random coincidences. The silicon detectors were carefully calibrated and the ion dependent pulse height deficits were taken into account.

These four experimental mass yield distributions are presented in figure 10. All distributions are normalised to 200%. In addition, the semi-empirical mass yield curve based on the Wahl model [46] is displayed. The data is taken from the OECD Nuclear Energy Agency UKFY4 data base [48]. The yields for 25 MeV proton-induced fission are achieved by linearly interpolating between the tabulated yields for 20 MeV and 30 MeV proton-induced fission.

It is readily seen that these mass yield distributions do not agree with each other. Slightly different proton energies in each experiment can be a partial reason of the differences, however, the disagreement of distribution in [6] is too large to be explained. The effort to deduce the independent fission yields in 25 MeV proton-induced fission utilising equation 2 was thus carried out separately for each experimental distribution.

4.2.2 Absolute independent isotopic yields

Before aiming to calculate the absolute independent fission yield, it has to be noted that not all the normalised isotopic yields $Y^n_{A,Z}$ were determined in the experiment. Gaps in the yield data need to be addressed.

Firstly, the experimental isotopic yields were replaced by Gaussian fits of the distributions, whose parameters are shown in figures 6 and 7. This covers missing isotopes and to some extent extrapolates towards the wings of the distribution. Secondly, the distributions for heavy elements (Z $>$ 57) were taken from the model of Rubchenya [44, 45] which seems to reproduce the data sufficiently well, except for elements 35 $<$ Z $<$ 45.

The set of scaling factors k_Z that would fulfil equation 2 was investigated separately for each mass yield distribution shown in figure 10. An additional restriction is that the charge of the complementary fission products must be conserved. In this requirement proton evaporation from the compound nucleus and ternary fission are neglected as rare processes. The results are shown in figures 11 and 12 for the mass yields from UKFY4 data base [48] and from Isaev *et al.* [6], respectively. In the legend of the figures the complementary elements whose total charge equals Z = 93 are placed on the same row. Note that the shown independent isotopic yield distributions in these figures are not the experimental ones but Gaussian approximations.

The displayed mass yield distributions are the two which differ most of the investigated ones. However, as seen from figures 11 and 12, such a set of scaling factors k_Z can be found for each of them that the quality of the fit, $\tilde{\chi}^2$, is roughly equal. Furthermore, after the factors k_Z have been adjusted so that the isotopic yields reproduce the mass yield distribution, the independent yields $Y_{A,Z}$ as well as the isobaric charge distributions $Y_A(Z)$ can be constructed. The expected width of charge distributions is $\sigma_Z \approx 0.70$ [12,18,41], as discussed above in section 3 in connection with krypton yields. The average width of the charge distributions from the data show in figures 11 and 12 $\sigma_Z = 0.717 \pm 0.092$ and 0.719 ± 0.095 for UKFY4 data base [48] and Isaev *et al.* [6] mass yields, respectively. The widths of the charge distributions that were constructed from isotopic yield distributions and a mass yield distribution thus agree with the experimental widths, known from the literature and supported by the current data. The same result was achieved for all investigated mass yield distributions [48,6,7,5] showing that no conclusions can be made on the accuracy of the mass yield distributions on the basis of the current isotopic yield data.

5 Conclusions

In this work the independent isotopic yield distributions in 25 MeV proton-induced fission of ^{nat}U were determined

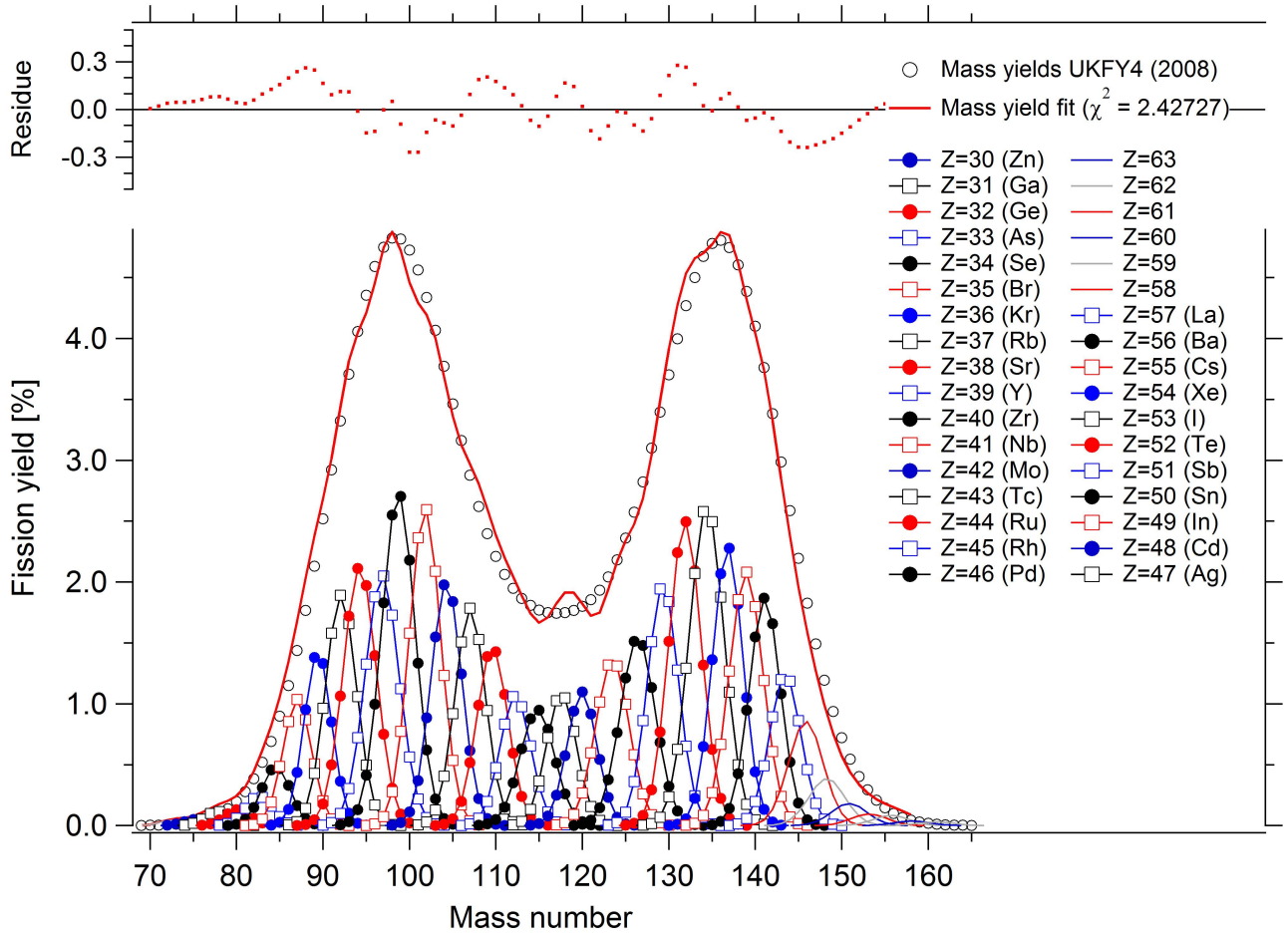

Fig. 11. The isotopic yield distributions in 25 MeV proton-induced fission, adjusted to the mass number yield distribution from [48].

for elements $30 \leq Z \leq 57$. In addition, tentative isotopic yield distributions were determined for elements $58 \leq Z \leq 61$. In 50 MeV proton-induced fission of ^{nat}U the isotopic yield distributions were determined for Zn (Z=30), Ga (Z=31), Rb (Z=35), Sr (Z=36), Zr (Z=40), Pd (Z = 46) and Cs (Z=55).

The yield distributions were compared to theoretical predictions of Rubchenya [44], Schmidt (GEF code) [51, 52] and the semiempirical model of Wahl [46,48]. The distribution centroids predicted by the GEF model were in better agreement with the data for 25 MeV proton-induced fission. The widths of the distributions were however predicted better by the Rubchenya model. Although the data were more sparse for 50 MeV proton-induced fission, it supported the GEF model predictions for the centroids and Rubchenya model for widhts as well. The experimental widths of the distributions were smaller than predicted by any of the models. The discrepancy from the models was most significant in the region of the symmetric fission. The Rubchenya model shows the best overall agreement with the experimental data.

An effort was made to combine the mass yields from literature with the isotopic yields determined in this work to find the independent fission yields in the 25 MeV proton-induced fission. Technically the isotopic yields could be combined with a mass yield distribution. This combination worked equally well for all mass yield distributions from the literature, which on the other hand do not agree with each other. The deduced independent yields thus strongly depend on the applied mass yield distribution. The accuracy of the mass yield distributions has to be determined separately, before the isotopic yields can reliably be converted to independent fission yields.

6 Acknowledgements

This work has been supported by the Academy of Finland under projects No. 139382 ("Precision Fission studies for Practical Needs"), No. 202256 and No. 111428, the Finnish Centre of Excellence Programme 2000-2005 (Project No. 44875, Nuclear and Condensed Matter Physics Programme at JYFL) and the Finnish Centre of Excellence Programme 2006-2011 (Project No. 213503, Nuclear and Accelerator Based Physics Programme at JYFL), and by European Union within EURISOL design study.

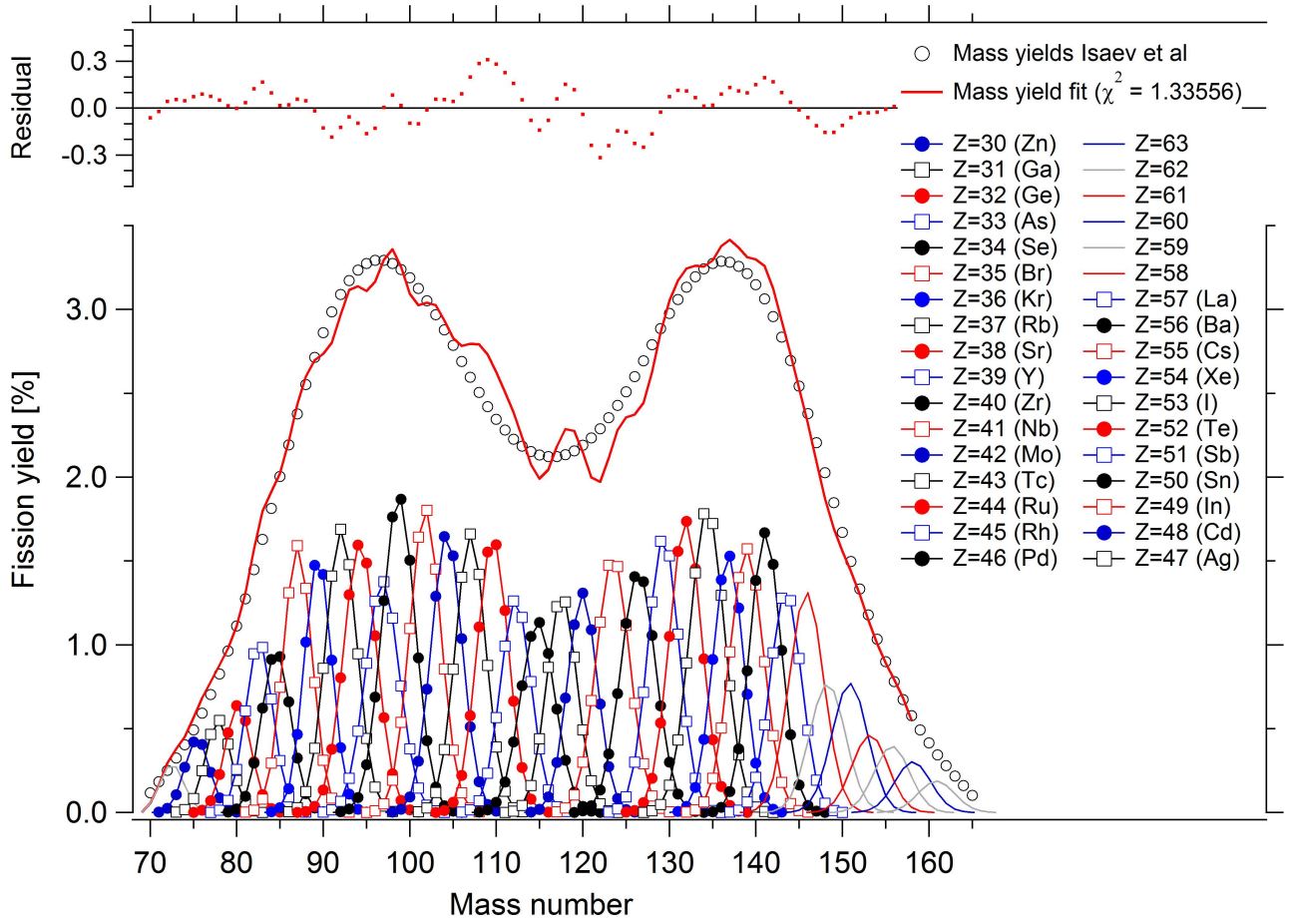

Fig. 12. The isotopic yield distributions in 25 MeV proton-induced fission, adjusted to the mass number yield distribution from [6].

References

1. I.D. Moore, T. Eronen, D. Gorelov, J. Hakala, A. Jokinen, A. Kankainen, V.S. Kolhinen, J. Koponen, H. Penttilä, I. Pohjalainen, M. Reponen, J. Rissanen, A. Saastamoinen, S. Rinta-Antila, V. Sonnenschein, and J. Äystö. Towards commissioning the new IGISOL-4 facility. *Nuclear Instruments and Methods in Physics Research Section B: Beam Interactions with Materials and Atoms*, 317, Part B(0):208 – 213, 2013. XVIth International Conference on Electro-Magnetic Isotope Separators and Techniques Related to their Applications, December 27, 2012 at Matsue, Japan.
2. EURISOL. http://www.eurisol.org/, 2008. [Online; accessed 10-Aug-2015].
3. The Generation IV international forum. Technology roadmap update for Generation IV nuclear energy systems. https://www.gen-4.org/gif/jcms/c_60729/technology-roadmap-update-2013, January 2014.
4. H.O. Denschag, T. R. England, A. A. Goverdovski, M. F. James, M. Lammer, Qichang Liang, Tingjin Liu, R. W. Mills, B. F. Rider, G. Rudstam, F. Storrer, A. C. Wahl, Dao Wang, and D. R. Weaver. *IAEA-TECDOC-1168, Compilation and evaluation of fission yield nuclear data, Final report of a co-ordinated research project 1991 - 1996*. IAEA, Vienna, 2000.
5. S. Baba, H. Umezawa, and H. Baba. Mass distribution and the total fission cross section in the fission of ^{238}U with protons of energies ranging between 13 and 55 MeV. *Nuclear Physics A*, 175(1):177 – 198, 1971.
6. S. Isaev, R. Prieels, Th. Keutgen, J. Van Mol, Y. El Masri, and P. Demetriou. Proton-induced fission on actinide nuclei at energies 27 and 63 MeV. *Nuclear Physics A*, 809(12):1 – 29, 2008.
7. V.A. Rubchenya, W.H. Trzaska, D.N. Vakhtin, J. Äystö, P. Dendooven, S. Hankonen, A. Jokinen, Z. Radivojevich, J.C. Wang, I.D. Alkhazov, A.V. Evsenin, S.V. Khlebnikov, A.V. Kuznetsov, V.G. Lyapin, O.I. Osetrov, G.P. Tiourin, A.A. Aleksandrov, and Yu.E. Penionzhkevich. Neutron and fragment yields in proton-induced fission of ^{238}U at intermediate energies. *Nuclear Instruments and Methods in Physics Research Section A: Accelerators, Spectrometers, Detectors and Associated Equipment*, 463(3):653 – 662, 2001. Accelerator driven systems.
8. J Äystö. Development and applications of the IGISOL technique. *Nuclear Physics A*, 693(12):477 – 494, 2001. Radioactive Nuclear Beams.
9. I.D. Moore, P. Dendooven, and J. Ärje. The IGISOL technique three decades of developments. *Hyperfine Interactions*, 223(1-3):17–62, 2014.

10. M. Leino, P. P. Jauho, J. Äystö, P. Decrock, P. Dendooven, K. Eskola, M. Huyse, A. Jokinen, J. M. Parmonen, H. Penttilä, G. Reusen, P. Taskinen, P. Van Duppen, and J. Wauters. Independent and cumulative yields of very neutron-rich nuclei in 20 MeV p - and 18 - 41 MeV d -induced fission of ^{238}U. *Phys. Rev. C*, 44:336–344, Jul 1991.
11. P. P. Jauho, A. Jokinen, M. Leino, J. M. Parmonen, H. Penttilä, J. Äystö, K. Eskola, and V. A. Rubchenya. Isotopic product distributions in the near symmetric mass region in proton induced fission of ^{238}U. *Phys. Rev. C*, 49:2036–2044, Apr 1994.
12. G. Lhersonneau, P. Dendooven, G. Canchel, J. Huikari, P. Jardin, A. Jokinen, V. Kolhinen, C. Lau, L. Lebreton, A.C. Mueller, A. Nieminen, S. Nummela, H. Penttilä, K. Peräjärvi, Z. Radivojevic, V. Rubchenya, M.-G. Saint-Laurent, W.H. Trzaska, D. Vakhtin, J. Vervier, A.C.C. Villari, J.C. Wang, and J. Äystö. Production of neutron-rich isotopes in fission of uranium induced by neutrons of 20 MeV average energy. *The European Physical Journal A - Hadrons and Nuclei*, 9(3):385–396, 2000.
13. K. Kruglov, A. Andreyev, B. Bruyneel, S. Dean, S. Franchoo, M. Gòrska, K. Helariutta, M. Huyse, Yu. Kudryavtsev, W.F. Mueller, N.V.S.V. Prasad, R. Raabe, K.-H. Schmidt, P. Van Duppen, J. Van Roosbroeck, K. Van de Vel, and L. Weissman. Yields of neutron-rich isotopes around z = 28 produced in 30 MeV proton-induced fission of ^{238}U. *The European Physical Journal A - Hadrons and Nuclei*, 14(3):365–370, 2002.
14. K. Kruglov, A. Andreyev, B. Bruyneel, S.S. Dean, S. Franchoo, M. Huyse, Y. Kudryavtsev, W.F. Mueller, N.V.S.V. Prasad, R. Raabe, I. Reusen, K.-H. Schmidt, K. Van de Vel, P. Van Duppen, J. Van Roosbroeck, and L. Weissman. Production of neutron-rich copper isotopes in 30-MeV proton-induced fission of ^{238}U. *Nuclear Physics A*, 701(14):145 – 149, 2002. 5th International Conference on Radioactive Nuclear Beams.
15. S. Franchoo, M. Huyse, K. Kruglov, Y. Kudryavtsev, W. F. Mueller, R. Raabe, I. Reusen, P. Van Duppen, J. Van Roosbroeck, L. Vermeeren, A. Wöhr, K.-L. Kratz, B. Pfeiffer, and W. B. Walters. Beta decay of $^{68-74}$Ni and level structure of neutron-rich Cu isotopes. *Phys. Rev. Lett.*, 81:3100–3103, Oct 1998.
16. W. F. Mueller, B. Bruyneel, S. Franchoo, H. Grawe, M. Huyse, U. Köster, K.-L. Kratz, K. Kruglov, Y. Kudryavtsev, B. Pfeiffer, R. Raabe, I. Reusen, P. Thirolf, P. Van Duppen, J. Van Roosbroeck, L. Vermeeren, W. B. Walters, and L. Weissman. Magicity of the ^{68}Ni semidouble-closed-shell nucleus probed by gamow-teller decay of the odd- A neighbors. *Phys. Rev. Lett.*, 83:3613–3616, Nov 1999.
17. H. Kudo, M. Maruyama, M. Tanikawa, M. Fujita, T. Shinozuka, and M. Fujioka. Transport efficiency of fission products in IGISOL. *Nuclear Instruments and Methods in Physics Research Section B: Beam Interactions with Materials and Atoms*, 126(14):209 – 212, 1997. International Conference on Electromagnetic Isotope Separators and Techniques Related to Their Applications.
18. H. Kudo, M. Maruyama, M. Tanikawa, T. Shinozuka, and M. Fujioka. Most probable charge of fission products in 24 mev proton induced fission of ^{238}U. *Phys. Rev. C*, 57:178–188, Jan 1998.
19. S. Goto, D. Kaji, H. Kudo, M. Fujita, T. Shinozuka, and M. Fujioka. Isomeric yield ratios of fission products in proton-induced fission of ^{232}Th. *Journal of Radioanalytical and Nuclear Chemistry*, 239(1):109–112, 1999.
20. L. Stroe, G. Lhersonneau, A. Andrighetto, P. Dendooven, J. Huikari, H. Penttilä, K. Peräjärvi, L. Tecchio, and Y. Wang. Production of neutron-rich nuclei in fission induced by neutrons generated by the $p + {}^{13}C$ reaction at 55 MeV. *Eur. Phys. J. A*, 17(1):57–63, 2003.
21. A. Astier, R. Beráud, A. Bouldjedri, R. Duffait, A. Emsallem, M. Meyer, S. Morier, P. Pangaud, N. Redon, D. Barnèoud, J. Blachot, J. Genevey, A. Gizon, R. Guglielmini, J. Inchaouh, G. Margotton, J.L. Vieux-Rochaz, J. Ärje, J. Äystö, P. Jauho, A. Jokinen, H. Penttilä, K. Eskola, M.E. Leino, and J.B. Marquette. Status report of the SARA IGISOL used in the study of the ^{238}U (α 40 MeV, f) reaction. *Nuclear Instruments and Methods in Physics Research Section B: Beam Interactions with Materials and Atoms*, 70(14):233 – 240, 1992.
22. M. Heffner, D.M. Asner, R.G. Baker, J. Baker, S. Barrett, C. Brune, J. Bundgaard, E. Burgett, D. Carter, M. Cunningham, J. Deaven, D.L. Duke, U. Greife, S. Grimes, U. Hager, N. Hertel, T. Hill, D. Isenhower, K. Jewell, J. King, J.L. Klay, V. Kleinrath, N. Kornilov, R. Kudo, A.B. Laptev, M. Leonard, W. Loveland, T.N. Massey, C. McGrath, R. Meharchand, L. Montoya, N. Pickle, H. Qu, V. Riot, J. Ruz, S. Sangiorgio, B. Seilhan, S. Sharma, L. Snyder, S. Stave, G. Tatishvili, R.T. Thornton, F. Tovesson, D. Towell, R.S. Towell, S. Watson, B. Wendt, L. Wood, and L. Yao. A time projection chamber for high accuracy and precision fission cross-section measurements. *Nuclear Instruments and Methods in Physics Research Section A: Accelerators, Spectrometers, Detectors and Associated Equipment*, 759:50 – 64, 2014.
23. A. Tsinganis, E. Berthoumieux, C. Guerrero, N. Colonna, M. Calviani, R. Vlastou, S. Andriamonje, V. Vlachoudis, F. Gunsing, C. Massimi, S. Altstadt, J. Andrzejewski, L. Audouin, M. Barbagallo, V. Bécares, F. Bečvá, F. Belloni, J. Billowes, V. Boccone, D. Bosnar, M. Brugger, F. Calvio, D. Cano-Ott, C. Carrapiço, F. Cerutti, M. Chin, G. Cortés, M.A. Cortés-Giraldo, M. Diakaki, C. Domingo-Pardo, I. Duran, R. Dressler, N. Dzysiuk, C. Eleftheriadis, A. Ferrari, K. Fraval, S. Ganesan, A.R. García, G. Giubrone, M.B. Gómez-Hornillos, I.F. Gonçalves, E. González-Romero, E. Griesmayer, P. Gurusamy, A. Hernández-Prieto, D.G. Jenkins, E. Jericha, Y. Kadi, and F. K˙ Measurement of the ^{242}Pu(n,f) cross section at the CERN nTOF Facility. *Nuclear Data Sheets*, 119:58 – 60, 2014.
24. D. Tarrío, L.S. Leong, L. Audouin, I. Duran, C. Paradela, L. Tassan-Got, S. Altstadt, J. Andrzejewski, M. Barbagallo, V. Becares, F. Bečvař, F. Belloni, E. Berthoumieux, J. Billowes, V. Boccone, D. Bosnar, M. Brugger, M. Calviani, F. Calvi no, D. Cano-Ott, C. Carrapiço, F. Cerutti, E. Chiaveri, M. Chin, N. Colonna, G. Cortés, M.A. Cortés-Giraldo, M. Diakaki, C. Domingo-Pardo, N. Dzysiuk, C. Eleftheriadis, A. Ferrari, K. Fraval, S. Ganesan, A.R. García, G. Giubrone, M.B. Gómez-Hornillos, I.F. Gonçalves, E. González-Romero, E. Griesmayer, C. Guerrero, F. Gunsing, P. Gurusamy, D.G. Jenkins, E. Jericha, Y. Kadi, and F. K˙ Fission fragment angular distribution

of ^{232}Th(n,f) at the CERN nTOF Facility. *Nuclear Data Sheets*, 119:35 – 37, 2014.
25. S. Panebianco, D. Doré, F. Farget, F.-R. Lecolley, G. Lehaut, T. Materna, J. Pancin, and T. Papaevangelou. FALSTAFF: a novel apparatus for fission fragment characterization. *EPJ Web of Conferences*, 69:00021, 2014.
26. O. Serot, C. Amouroux, A. Bidaud, N. Capellan, S. Chabod, A. Ebran, H. Faust, G. Kessedjian, and U. K˙Recent results from lohengrin on fission yields and related decay properties. *Nuclear Data Sheets*, 119:320 – 323, 2014.
27. H. Penttilä. The layout of the IGISOL-3 facility. *Hyperfine Interactions*, 223(1-3):5–16, 2014.
28. T. Eronen, V.S. Kolhinen, V.-V. Elomaa, D. Gorelov, U. Hager, J. Hakala, A. Jokinen, A. Kankainen, P. Karvonen, S. Kopecky, I.D. Moore, H. Penttil/"a, S. Rahaman, S. Rinta-Antila, J. Rissanen, A. Saastamoinen, J. Szerypo, C. Weber, and J. Äystö. JYFLTRAP: a Penning trap for precision mass spectroscopy and isobaric purification. *The European Physical Journal A*, 48(4), 2012.
29. H. Penttilä, P. Karvonen, T. Eronen, V.-V. Elomaa, U. Hager, J. Hakala, A. Jokinen, A. Kankainen, I.D. Moore, K. Peräjärvi, S. Rahaman, S. Rinta-Antila, V. Rubchenya, A. Saastamoinen, T. Sonoda, and J. Äystö. Determining isotopic distributions of fission products with a Penning trap. *The European Physical Journal A*, 44(1):147–168, 2010.
30. H. Penttilä, V.-V. Elomaa, T. Eronen, J. Hakala, A. Jokinen, A. Kankainen, I.D. Moore, S. Rahaman, S. Rinta-Antila, J. Rissanen, V. Rubchenya, A. Saastamoinen, C. Weber, and J. Äystö. Fission yield studies at the IGISOL facility. *The European Physical Journal A*, 48(4), 2012.
31. H. Penttilä, D. Gorelov, P. Karvonen, V.-V. Elomaa, T. Eronen, J. Hakala, A. Jokinen, A. Kankainen, I.D. Moore, J. Parkkonen, S. Rahaman, S. Rinta-Antila, J. Rissanen, V. Rubchenya, T. Sonoda, J. Äystö, M. Lantz, A. Mattera, V.D. Simutkin, S. Pomp, and I. Ryzhov. Independent isotopic product yields in 25 MeV and 50 MeV charged particle induced fission of ^{238}U and ^{232}Th. *Nuclear Data Sheets*, 119:334 – 337, 2014.
32. P. Karvonen and I.D. Moore and T. Sonoda and T. Kessler and H. Penttilä and K. Peräjärvi and P. Ronkanen and J. Äystö. A sextupole ion beam guide to improve the efficiency and beam quality at IGISOL. *Nuclear Instruments and Methods in Physics Research Section B: Beam Interactions with Materials and Atoms*, 266(21):4794 – 4807, 2008.
33. A. Nieminen, J. Huikari, A. Jokinen, J. Äystö, P. Campbell, and E.C.A. Cochrane. Beam cooler for low-energy radioactive ions. *Nuclear Instruments and Methods in Physics Research Section A: Accelerators, Spectrometers, Detectors and Associated Equipment*, 469(2):244 – 253, 2001.
34. A. Nieminen, P. Campbell, J. Billowes, D. H. Forest, J. A. R. Griffith, J. Huikari, A. Jokinen, I. D. Moore, R. Moore, G. Tungate, and J. Äystö. On-line ion cooling and bunching for collinear laser spectroscopy. *Phys. Rev. Lett.*, 88:094801, Feb 2002.
35. A. Nieminen, P. Campbell, J. Billowes, D.H. Forest, J.A.R. Griffith, J. Huikari, A. Jokinen, I.D. Moore, R. Moore, G. Tungate, and J. Äystö. Cooling and bunching of ion beams for collinear laser spectroscopy. *Nuclear Instruments and Methods in Physics Research Section B: Beam Interactions with Materials and Atoms*, 204(0):563 – 569, 2003. 14th International Conference on Electromagnetic Isotope Separators and Techniques Related to their Applications.
36. G. Gabrielse. The true cyclotron frequency for particles and ions in a penning trap. *International Journal of Mass Spectrometry*, 279(23):107 – 112, 2009.
37. G. Savard, St. Becker, G. Bollen, H.-J. Kluge, R.B. Moore, Th. Otto, L. Schweikhard, H. Stolzenberg, and U. Wiess. A new cooling technique for heavy ions in a penning trap. *Physics Letters A*, 158(5):247 – 252, 1991.
38. V.S. Kolhinen, S. Kopecky, T. Eronen, U. Hager, J. Hakala, J. Huikari, A. Jokinen, A. Nieminen, S. Rinta-Antila, J. Szerypo, and J. Äystö. JYFLTRAP: a cylindrical Penning trap for isobaric beam purification at IGISOL. *Nuclear Instruments and Methods in Physics Research Section A: Accelerators, Spectrometers, Detectors and Associated Equipment*, 528(3):776 – 787, 2004.
39. Yu. Kudryavtsev, T.E. Cocolios, J. Gentens, O. Ivanov, M. Huyse, D. Pauwels, M. Sawicka, T. Sonoda, P. Van den Bergh, and P. Van Duppen. Characterization of the LISOL laser ion source using spontaneous fission of ^{252}Cf. *Nuclear Instruments and Methods in Physics Research Section B: Beam Interactions with Materials and Atoms*, 266(1920):4368 – 4372, 2008. Proceedings of the XVth International Conference on Electromagnetic Isotope Separators and Techniques Related to their Applications.
40. S. J. Genuis, D. Birkholz, I. Rodushkin, and S. Beesoon. Blood, urine, and sweat (BUS) study: Monitoring and elimination of bioaccumulated toxic elements. *Archives of Environmental Contamination and Toxicology*, 61(2):344–357, 2011.
41. J. A. McHugh and M. C. Michel. Fission-fragment mass and charge distribution for the moderately excited U^{236} compound nucleus. *Phys. Rev.*, 172:1160–1175, Aug 1968.
42. M. Tanikawa, H. Kudo, H. Sunaoshi, M. Wada, T. Shinozuka, and M. Fujioka. Isomeric yield ratios of fission products in the system of 24 MeV proton-induced fission of ^{238}U. *Zeitschrift für Physik A Hadrons and Nuclei*, 347(1):53–62, 1993.
43. B. L. Tracy, J. Chaumont, R. Klapisch, J. M. Nitschke, A. M. Poskanzer, E. Roeckl, and C. Thibault. Rb and Cs isotopic cross sections from 40-60-MeV-Proton fission of ^{238}U, ^{232}Th, and ^{235}U. *Phys. Rev. C*, 5:222–234, Jan 1972.
44. V. A. Rubchenya. Prompt fission neutron emission in neutron and proton induced reactions at intermediate energies. *Phys. Rev. C*, 75:054601, May 2007.
45. V.A. Rubchenya and J. Äystö. Consistent theoretical model for the description of the neutron-rich fission product yields. *The European Physical Journal A*, 48(4), 2012.
46. A.C. Wahl. *Systematics of Fission-Product Yields.* May 2002.
47. A.C. Wahl. *Fission product Yield Data for the Transmutation of Minor Actinide Nuclear Waste*, chapter 4.2., pages 117 – 148. Number STI/PUB/1286. IAEA, April 2008.
48. Robert Mills. UKFY4.1 library and documentation. http://www.oecd-nea.org/dbdata/jeff/decay/, 2008. [Online; accessed 20-May-2015].
49. D.M.Gorodisskiy, S. I. Mulgin, A. Yu. Rusanov, and S. V. Zhdanov. *Fission product Yield Data for the Transmutation of Minor Actinide Nuclear Waste*, chapter 4.5., pages 183 – 209. Number STI/PUB/1286. IAEA, April 2008.

50. A. C. Wahl, R. L. Ferguson, D. R. Nethaway, D. E. Troutner, and K. Wolfsberg. Nuclear-charge distribution in low-energy fission. *Phys. Rev.*, 126:1112–1127, May 1962.
51. K. H. Schmidt, B. Jurado, and C. Amouroux. General Description of Fission Observables - GEF Model. Technical Report NEA/DB/DOC(2014)1, OECD Nuclear Energy Agency, 2014.
52. K.-H. Schmidt, B. Jurado, C. Amouroux, and C. Schmitt. General description of fission observables: {GEF} model code. *Nuclear Data Sheets*, 131:107 – 221, 2016. Special Issue on Nuclear Reaction Data.
53. K.-H. Schmidt. GEF 2015/2.2 download website. http://www.khs-erzhausen.de/GEF-2015-2-2.html, September 2015.